NPS-53-90-005

NAVAL POSTGRADUATE SCHOOL

Monterey, California

BUOYANT CONVECTION IN DENDRITIC SOLIDIFICATION

D. CANRIGHT
S. H. DAVIS

April 4, 1990

Prepared for:
Naval Postgraduate School
Monterey, California 93943

NASA Microgravity Science and
Applications Program

NAVAL POSTGRADUATE SCHOOL
MONTEREY, CA 93943

Rear Admiral R. W. West, JR
Superintendent

Harrison Shull
Provost

This report was prepared in conjunction with research conducted for the Naval Postgraduate School and funded by the Naval Postgraduate School.

Prepared by:

DAVID CANRIGHT
Assistant Professor

Reviewed by:

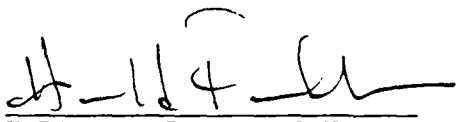

HAROLD M. FREDRICKSEN
Chairman
Department of Mathematics

Released by:

G. E. SCHACHER
Dean of Faculty and Graduate Education

SECURITY CLASSIFICATION OF THIS PAGE

REPORT DOCUMENTATION PAGE

Form Approved
OMB No 0704-0188

1a REPORT SECURITY CLASSIFICATION UNCLASSIFIED	1b RESTRICTIVE MARKINGS
2a SECURITY CLASSIFICATION AUTHORITY	3 DISTRIBUTION / AVAILABILITY OF REPORT Approved for public release; distribution unlimited
2b DECLASSIFICATION / DOWNGRADING SCHEDULE	
4 PERFORMING ORGANIZATION REPORT NUMBER(S) NPS-53-90-005	5 MONITORING ORGANIZATION REPORT NUMBER(S) NPS-53-90-005
6a NAME OF PERFORMING ORGANIZATION Naval Postgraduate School 6b OFFICE SYMBOL (If applicable) MA	7a NAME OF MONITORING ORGANIZATION Naval Postgraduate School
6c ADDRESS (City, State, and ZIP Code) Monterey, CA 93943	7b ADDRESS (City, State, and ZIP Code) Monterey, CA 93943
8a NAME OF FUNDING / SPONSORING ORGANIZATION Naval Postgraduate School 8b OFFICE SYMBOL (If applicable) MA	9 PROCUREMENT INSTRUMENT IDENTIFICATION NUMBER O&MN, Direct Funding
8c ADDRESS (City, State, and ZIP Code) Monterey, CA 93943	10 SOURCE OF FUNDING NUMBERS PROGRAM ELEMENT NO / PROJECT NO / TASK NO / WORK UNIT ACCESSION NO

11 TITLE (Include Security Classification)
BUOYANT CONVECTION IN DENDRITIC SOLIDIFICATION

12 PERSONAL AUTHOR(S)
David Canright and S. H. Davis

13a TYPE OF REPORT	13b TIME COVERED	14 DATE OF REPORT (Year, Month, Day)	15 PAGE COUNT
Technical Report	FROM 1/88 TO 1/90	April 4, 1990	37

16 SUPPLEMENTARY NOTATION

17 COSATI CODES			18 SUBJECT TERMS (Continue on reverse if necessary and identify by block number)
FIELD	GROUP	SUB-GROUP	
			Dendrite, Solidification, Ivantsov, Buoyant Convection

19 ABSTRACT (Continue on reverse if necessary and identify by block number)

In solidification, when the process is limited by diffusion of released latent heat or solute, often the two-phase interface forms finger-like shapes called dendrites, whose tips are nearly paraboloidal in form. For a pure material solidifying into an undercooled melt, if surface energy and gravity are negligible, a well-known solution due to Ivantsov (1947) describes the steady growth with a paraboloidal interface. We construct a regular perturbation to this solution for a downward growing axisymmetric dendrite, based on the smallness of a buoyancy parameter G, to examine the effects of buoyant flow on the solidification. The analytic solution predicts that generally the buoyancy enhances growth and changes the shape of the interface, giving a sharper tip and wider base. These effects depend strongly on the Prandtl number, and also on the Stefan number (undercooling). The results compare well with the experiments of Huang and Glicksman (1981a) up to G 5000, but overpredict convective effects for higher G.

20 DISTRIBUTION / AVAILABILITY OF ABSTRACT	21 ABSTRACT SECURITY CLASSIFICATION
☒ UNCLASSIFIED/UNLIMITED ☐ SAME AS RPT ☐ DTIC USERS	UNCLASSIFIED
22a NAME OF RESPONSIBLE INDIVIDUAL David Canright	22b TELEPHONE (Include Area Code) (408) 646-2782 22c OFFICE SYMBOL MA/Ca

DD Form 1473, JUN 86 Previous editions are obsolete SECURITY CLASSIFICATION OF THIS PAGE

S/N 0102-LF-014-6603

BUOYANT CONVECTION IN DENDRITIC SOLIDIFICATION

D. Canright
Mathematics Dept., Code 53Ca
Naval Postgraduate School
Monterey, CA 93943

S. H. Davis
Engineering Sciences & Applied Mathematics
The Technological Institute
Northwestern University
Evanston, IL 60208

ABSTRACT

In solidification, when the process is limited by diffusion of released latent heat or solute, often the two-phase interface forms finger-like shapes called dendrites, whose tips are nearly paraboloidal in form. For a pure material solidifying into an undercooled melt, if surface energy and gravity are negligible, a well-known solution due to Ivantsov (1947) describes the steady growth with a paraboloidal interface. We construct a regular perturbation to this solution for a downward growing axisymmetric dendrite, based on the smallness of a buoyancy parameter G, to examine the effects of buoyant flow on the solidification. The analytic solution predicts that generally the buoyancy enhances growth and changes the shape of the interface, giving a sharper tip and wider base. These effects depend strongly on the Prandtl number, and also on the Stefan number (undercooling). The results compare well with the experiments of Huang and Glicksman (1981a) up to $G \sim 5000$, but overpredict convective effects for higher G.

BUOYANT CONVECTION IN DENDRITIC SOLIDIFICATION

INTRODUCTION

Solidification processes are important in a variety of contexts, and are of particular interest in the processing of materials. The small-scale details of the solidification can affect the resulting microstructure, and hence the bulk properties, of the final product. This practical context has led to a great deal of research toward understanding the details of solidification processes.

In many typical solidification situations, an initially smooth solid surface becomes morphologically unstable as it grows; small bumps grow into long fingers, which in turn grow side branches, yielding a tree-like stucture called a dendrite. Experiments have shown that the growing tip of the dendrite is closely approximated by an axisymmetric paraboloid for many materials (or an elliptic paraboloid for some others).

The present work deals with the effects on this growing dendrite tip of buoyant flow in the molten phase, driven by the release of latent heat upon solidification. (With the possibility of processing materials in a microgravity environment, prediction of gravitational effects takes on practical importance.) To gain some insight into the effects of buoyancy on dendritic solidification while keeping the analysis tractable, the simplest situation is considered; we analyze an isolated axisymmetric dendrite growing downward into an undercooled, pure melt, when buoyantly induced velocities are small compared to the speed of the solidification front and surface energy is negligible. We find a solution in the form of a regular perturbation expansion in the small gravitational parameter (G); the solution shows explicitly the dependence upon the Prandtl number (P) and the Stefan number (S, the dimensionless undercooling).

There has been much previous work on dendrites with convection, although a relatively small proportion applies directly to natural convection near isolated dendrites. The experimental study by Huang and Glicksman (1981a,b) using succinonitrile shows that buoyant convection can significantly affect both the growth speed and the tip radius of isolated dendrites, when the growth is relatively slow. They found that a dendrite growing downward grew faster, with a smaller tip, than one growing upward in the same conditions. Similar experiments by Tirmizi and Gill (1987), for an ice-water system, shows qualitatively similar results with platelike dendrites, and with down and up switched due to water's increasing density with temperature near freezing.

Ananth and Gill (1988) present a theoretical analysis of the same problem considered here, but with a different simplifying approximation, giving a different region of applicability. They assume the dendrite is a paraboloid, and essentially apply a coordinate expansion, formally valid within a fraction of a tip radius from the very tip. They derive a pair of coupled nonlinear ordinary differential equations which include the nonlinear effects of buoyancy in this region, which they solve numerically for some choices of the parameters. In contrast, we assume the buoyancy is relatively small in order to use an expansion in the gravitational parameter about the known paraboloidal solution (Ivantsov, 1947). This linearizes the buoyant convection effects, which allows for an explicit analytic solution showing all parameter dependence, formally valid within many tip radii from the very tip. This solution predicts that buoyancy affects not only the growth Peclet number

(Pe, the dimensionless product of growth speed and dendrite tip size) of the dendrite, but also its shape; the perturbed dendrite is not paraboloidal.

PROBLEM STATEMENT

Consider a smooth dendrite of a pure substance, growing into an undercooled quiescent melt. We assume the dendrite is axisymmetric, with the axis vertical, growing downward (see Figure 1), and that the growth is steady in the reference frame of the solid-liquid interface. Surface energy and non-equilibrium effects at the interface are neglected, so the liquid solidifies at the equilibrium melting temperature T_m; as a result, the entire solid phase is isothermal, at T_m. The material properties in each phase are assumed constant, with no density change upon solidification. The Boussinesq approximation is applied in the melt. Then the governing equations in the melt are the conservation of energy, mass, and momentum:

$$\mathbf{u} \cdot \nabla T = \kappa \nabla^2 T \quad , \tag{1}$$

$$\nabla \cdot \mathbf{u} = 0 \quad , \tag{2}$$

$$(\mathbf{u} \cdot \nabla)\mathbf{u} = -\frac{1}{\rho}\nabla p + \nu \nabla^2 \mathbf{u} - \alpha(T - T_\infty)\mathbf{g} \quad , \tag{3}$$

with the boundary conditions

$$\text{at the interface:} \qquad T = T_m \quad , \tag{4}$$

$$\mathbf{u} = V\hat{\mathbf{z}} \quad , \tag{5}$$

$$-\rho L\, V\hat{\mathbf{z}} \cdot \hat{\mathbf{n}} = -k(\nabla T) \cdot \hat{\mathbf{n}} \quad , \tag{6}$$

$$\text{deep into the fluid:} \qquad T \to T_\infty \quad , \tag{7}$$

$$\mathbf{u} \to V\hat{\mathbf{z}} \quad , \tag{8}$$

where T is the temperature, T_m is the equilibrium melting temperature, T_∞ is the (undercooled) temperature of the undisturbed melt, κ is the thermal diffusivity, k is the thermal conductivity, α is the thermal expansion coefficient, L is the latent heat (per unit mass), $\mathbf{u}$ is the velocity (relative to the interface), V is the axial growth speed of the dendrite (to be determined in the solution), ρ is the density, p is the reduced pressure, ν is the kinematic viscosity, g is the acceleration of gravity, $\hat{\mathbf{z}}$ is a unit vector upward, and $\hat{\mathbf{n}}$ is a unit vector normal to the interface (outward). Condition (6) says that the latent heat released at the interface must be removed by conduction into the melt, while (5) and (8) say that the solid and the undisturbed melt are motionless in the laboratory reference frame.

To nondimensionalize the problem, a length or velocity scale is required. Near the dendrite tip, the relevant length scales are the tip radius R, the thermal boundary layer thickness κ/V, and the viscous boundary layer thickness ν/V. All of these involve one of the unknowns, either tip radius R or growth speed V. As a result, the dimensionless solution predicts the growth Peclet number $Pe = RV/2\kappa$, but cannot predict R and V separately. This problem, of selecting which of a family of solutions is realized in nature, is inherent in the problem as posed (due to the neglect of surface energy), and is common

to the orginal (non-buoyant) solution of Ivantsov (1947), the analysis of Ananth and Gill (1988), and the present work. For a unique physical solution, an additional selection criterion is needed, e.g., based on the morphological stability of the dendrite tip.

We nondimensionalize the temperature by $\tilde{T} = (T - T_\infty)/(T_m - T_\infty)$, the velocity by $\tilde{\mathbf{u}} = \mathbf{u}/V$, and lengths by the thermal boundary layer thickness $\tilde{\mathbf{x}} = \mathbf{x}/(\kappa/V)$, then drop the tildes. We introduce an axisymmetric stream function Ψ to conserve mass, and use a vorticity formulation to eliminate the pressure. Then the dimensionless equations for energy, stream function, and vorticity are

$$\mathbf{u} \cdot \nabla T = \nabla^2 T \quad , \tag{9}$$

$$\boldsymbol{\omega} = -\nabla^2 \left(\frac{\Psi}{r} \hat{\boldsymbol{\phi}} \right) \quad , \tag{10}$$

$$(\mathbf{u} \cdot \nabla)\boldsymbol{\omega} - (\boldsymbol{\omega} \cdot \nabla)\mathbf{u} = P\nabla^2 \boldsymbol{\omega} - G \frac{\partial T}{\partial r} \hat{\boldsymbol{\phi}} \quad , \tag{11}$$

with the boundary conditions

$$\text{at the interface:} \quad T = 1 \quad , \tag{12}$$

$$\Psi = r^2/2 \quad , \tag{13}$$

$$\nabla \Psi = r\, \hat{\mathbf{r}} \quad , \tag{14}$$

$$\hat{\mathbf{z}} \cdot \hat{\mathbf{n}} = S(\nabla T) \cdot \hat{\mathbf{n}} \quad , \tag{15}$$

$$\text{deep into the fluid:} \quad T \to 0 \quad , \tag{16}$$

$$\Psi \to r^2/2 \quad , \tag{17}$$

where

$$\mathbf{u} = \nabla \times \left(\frac{\Psi}{r} \hat{\boldsymbol{\phi}} \right) \quad , \qquad \boldsymbol{\omega} = \nabla \times \mathbf{u} \quad , \tag{18}$$

(r, ϕ, z) are cylindrical coordinates with corresponding unit vectors $\hat{\mathbf{r}}$, $\hat{\boldsymbol{\phi}}$, $\hat{\mathbf{z}}$, and the three dimensionless parameters are Stefan number (undercooling) $S \equiv (T_m - T_\infty)C_p/L$, Prandtl number $P \equiv \nu/\kappa$, and a gravitational parameter $G \equiv g\alpha(T_m - T_\infty)\kappa/V^3$ (like a Grashof number times Prandtl number squared), and C_p is the specific heat. The undercooling S must be smaller than 1 for the rate of solidification to be limited by thermal diffusion, as assumed here; otherwise, the solidification is very rapid and attachment kinetics limit growth.

The problem formulated above, of solidification of a pure substance into an undercooled melt, limited by diffusion of released latent heat, is analogous to a solidification problem for a binary alloy, under certain assumptions. For a two-component mixture, the solid and liquid phases in local thermodynamic equilibrium at the interface generally have different compositions. For example, considering the major component the solvent and the other the solute, typically the solute is less soluble in the solid phase, i.e., its concentration is smaller in the solid than in the liquid. Thus, as solidification proceeds, not only is latent heat released, but also the excess solute. When the mass diffusivity D is much smaller than the thermal diffusivity κ (the usual case) and the latent heat L is not large, then the

speed of solidification is limited by diffusion of the rejected solute into the melt, and the process is nearly isothermal.

Formally, if latent heat and thermal variations are negligible, then this alloy problem reduces to the identical dimensionless form above, with the following correspondences: $T \to C$, $\kappa \to D$, $S \to (C_l - C_\infty)/(C_l - C_s)$, $P \to Sc \equiv \nu/D$, $G \to g\beta(C_l - C_\infty)D/V^3$, where C is concentration of solute, with values C_s in the solid, C_l in the liquid at the interface, and C_∞ deep into the melt, D is the diffusivity of the solute in the melt, Sc is the Schmidt number, and β is a solutal coefficient of expansion, defined by $(\rho - \rho_\infty)/\rho_\infty = \beta(C - C_\infty)$. Therefore, the perturbation solution derived below applies to this binary solidification problem controlled by mass diffusion, as well as the case of a pure substance.

PERTURBATION SOLUTION

This problem presents several difficulties: the interface between the solid and liquid phases is a free boundary, the energy flux condition at the interface (15) is nonlinear, and the convection terms in the transport equations (9) and (10) are nonlinear. However, when buoyancy is negligible ($G \to 0$), a solution is well known, due to Ivantsov (1947). In this case, there is no motion of material (in the reference frame of the quiescent melt), and the solid-liquid interface is a paraboloid of revolution, moving steadily along its axis as the liquid solidifies. In the reference frame of the interface, the flow is uniform everywhere ($\mathbf{u} = \hat{\mathbf{z}}$).

To get some indication of the effects of gravity while avoiding the difficulties of the nonlinear convection terms, we consider the case where buoyancy is relatively small ($G \ll 1$), and seek a solution as a small perturbation to the Ivantsov solution.

The equations suggest a regular perturbation in G:

$$\begin{aligned} T &= T_0 + G\,T_1 + \cdots \quad , \\ \Psi &= \Psi_0 + G\,\Psi_1 + \cdots \quad , \\ \omega &= \omega_0 + G\,\omega_1 + \cdots \quad . \end{aligned} \tag{19}$$

Then the lowest order quantities are the Ivantsov solution, which is most easily expressed in paraboloidal coordinates (ξ, η, ϕ) (see Figure 2), where

$$\xi = \frac{\sqrt{r^2 + z^2} + z}{2} \quad , \qquad \eta = \frac{\sqrt{r^2 + z^2} - z}{2} \quad , \tag{20}$$

$$\text{so that } r = 2\sqrt{\xi\eta} \quad , \qquad z = \xi - \eta \quad ,$$

and ϕ is the azimuthal angle. (For comparison, these are not the same parabolic coordinates as in Ananth and Gill, 1988.) The thermal field and uniform flow are

$$T_0 = \frac{E_1(\eta)}{E_1(H_0)} \quad , \qquad \Psi_0 = \frac{r^2}{2} = 2\xi\eta \quad , \qquad \omega_0 = 0 \quad , \tag{21}$$

and the position of the interface is given by

$$\eta = H_0 \quad , \text{ such that: } H_0\, e^{H_0} E_1(H_0) = S \quad , \tag{22}$$

i.e., to lowest order the interface is a paraboloid whose dimensionless size (or Peclet number: $Pe = H_0 = RV/2\kappa$, R is the tip radius) is determined by the undercooling S. (This solution thus represents a whole family of physical solutions with V and R varying inversely; as mentioned above, an additional selection criterion is needed for a unique solution.)

We explicitly consider buoyant effects on the shape of the dendrite by expanding the interface position also in a regular perturbation in G:

$$\eta = H(\xi) = H_0 + GH_1(\xi) + \cdots \quad , \tag{23}$$

Here E_1 is a standard exponential integral:

$$E_n(x) \equiv \int_1^\infty \frac{e^{-xs}}{s^n} ds \quad .$$

At the next order, we first see the effects of buoyancy. Linearizing about the lowest order solution, the equations, in parabolic coordinates, become:

$$\xi \frac{\partial T_1}{\partial \xi} - \eta \frac{\partial T_1}{\partial \eta} - \frac{1}{2} \frac{\partial \Psi_1}{\partial \xi} T_0' = \frac{\partial}{\partial \xi}\left(\xi \frac{\partial T_1}{\partial \xi}\right) + \frac{\partial}{\partial \eta}\left(\eta \frac{\partial T_1}{\partial \eta}\right) \quad , \tag{24}$$

$$\omega_1 = \frac{-1}{2(\xi+\eta)\sqrt{\xi\eta}} \left[\xi \frac{\partial^2 \Psi_1}{\partial \xi^2} + \eta \frac{\partial^2 \Psi_1}{\partial \eta^2}\right] \quad , \tag{25}$$

$$\xi \frac{\partial \omega_1}{\partial \xi} - \eta \frac{\partial \omega_1}{\partial \eta} = P\left[\sqrt{\xi} \frac{\partial^2}{\partial \xi^2}(\sqrt{\xi}\,\omega_1) + \sqrt{\eta} \frac{\partial^2}{\partial \eta^2}(\sqrt{\eta}\,\omega_1)\right] - \sqrt{\xi\eta}\, T_0' \quad , \tag{26}$$

with the boundary conditions

$$\text{at } \eta = H_0: \qquad T_1 + H_1 T_0' = 0 \quad , \tag{27}$$

$$\Psi_1 = \frac{\partial \Psi_1}{\partial \eta} = 0 \quad , \tag{28}$$

$$H_1 + \xi H_1' = -S\left[H_1 T_0' + H_1 H_0 T_0'' + H_0 \frac{\partial T_1}{\partial \eta}\right] \quad , \tag{29}$$

$$\text{as } \eta \to \infty: \qquad T_1 \to 0 \quad , \qquad \Psi_1 \to 0 \quad , \tag{30}$$

where primes denote ordinary derivatives, and the interface conditions have been transferred to $\eta = H_0$ by expanding T and Ψ in Taylor series in η about H_0.

The flow at this order is driven only by the lowest order temperature gradient. So we can solve for the perturbation flow first, from (25), (26), (28), and (30b), then use the flow to find the temperature and interface shape perturbations.

Because the driving temperature gradient (T_0') depends only on one coordinate (η) and the interface conditions are prescribed on a coordinate surface ($\eta = H_0$), we seek a solution that is separable in parabolic coordinates. Assuming the vorticity is of the form

$$\omega_1(\xi, \eta) = \sqrt{\frac{\xi}{\eta}}\, f(\eta) \quad , \tag{31}$$

then the vorticity equation (26) becomes

$$P f'' + f' - \frac{f}{\eta} = T_0' = \frac{-e^{-\eta}}{\eta E_1(H_0)} \quad . \tag{32}$$

The general solution is

$$\omega_1 = \frac{1}{(1-P)E_1(H_0)} \sqrt{\frac{\xi}{\eta}} \left[E_2(\eta) + A\, E_2(\frac{\eta}{P}) + B\,\eta \right] \quad , \tag{33}$$

where A and B are arbitrary constants, and E_2 is an exponential integral.

The corresponding stream function is not in simple separable form, due to the combination $(\xi + \eta)$ in the denominator of the coefficient in (25). (That factor arises from the metric coefficients in paraboloidal coordinates.) However, assuming a stream function of the form

$$\Psi_1(\xi, \eta) = \xi^2 g(\eta) + \xi h(\eta) \quad , \tag{34}$$

then (25) becomes

$$\eta\, g'' = -2f \quad , \tag{35}$$

$$\eta\, h'' = -2(\eta f + g) \quad , \tag{36}$$

and the general solution is

$$\Psi_1 = \frac{-2}{(1-P)E_1(H_0)} \{\xi^2 [g_1(\eta) + AP g_1(\frac{\eta}{P}) + B\frac{\eta^2}{2} + C\eta + D] + \xi[h_1(\eta) + AP^2 h_1(\frac{\eta}{P}) - C\eta^2 + 2D\eta(1 - \log\eta) + E\eta + F]\} \quad . \tag{37}$$

where $g_1(\eta) \equiv E_2(\eta) - E_3(\eta)$, $h_1(\eta) \equiv 2E_3(\eta) - E_2(\eta)$, and A, B, C, D, E, and F are arbitrary constants (A and B the same as in (33)).

The boundary conditions on the separable parts $g(\eta)$ and $h(\eta)$ (i.e., the two functions in square brackets above) are

$$\text{at } \eta = H_0: \qquad g = g' = 0 \quad , \qquad h = h' = 0 \quad , \tag{38}$$

$$\text{as } \eta \to \infty: \qquad g \to 0 \quad , \qquad h \to 0 \quad . \tag{39}$$

Unfortunately, no choice of the six arbitrary constants can satisfy these six conditions, because most of the terms do not decay as $\eta \to \infty$. Only the first two terms in each set of brackets decay, and discarding the other terms to satisfy conditions far away (39) leaves only one free constant, A. Conversely, we can satisfy no slip and no penetration at the interface (38), but the resulting perturbation flow grows without bound away from the interface. Moreover, whatever solution we get will grow without bound in ξ, i.e., along the dendrite far from the tip. (Looking for more general homogeneous separable solutions to add on will not help; they will not have the right asymptotic form as $\xi \to \infty$.)

Clearly, a solution of the above form cannot be uniformly valid in space. However, we can find a *locally* valid solution that satisfies the interface conditions. This solution is valid within a (dimensionless) distance of $O(G^{-1})$ from the tip in all directions; we call this the *tip solution*. (See Figure 3.) Along the dendrite, far from the tip, the nonlinear effects of buoyant convection become important. We expect a strongly convecting boundary-layer in this region, but as it is far downstream from the tip, it should have negligible effects in the tip region. Far from the dendrite, a distance of $O(G^{-1})$, is well outside the thermal and viscous boundary layers (unless $P \sim G^{-1}$). In this outer region, the fluid is isothermal ($T = 0$) and the flow is irrotational; it matches the inner flow to the uniform flow of the undisturbed fluid. That is, far from the dendrite, the (potential) flow departs from separable form to conserve mass. So we seek a local solution about the tip that becomes potential flow far away.

We choose $B = 0$ so the vorticity decays in η. The corresponding terms represent Pouiselle pipe flow, without the pipe ($\mathbf{u} = r^2\hat{\mathbf{z}}$). We also choose $C = 0$ because the corresponding terms, which represent stagnation point flow ($\mathbf{u} = -r\hat{\mathbf{r}} + 2z\hat{\mathbf{z}}$), grow faster in η than the remaining terms. Another reason to discard the flow terms with coefficients B and C is that they would imply that the dendrite induces strong flow far ahead of the tip, which is physically unreasonable.

Then the other constants are given by the interface conditions (38):

$$\begin{aligned} A &= \frac{-g_1'(H_0)}{g_1'(H_0/P)} \quad , \\ D &= -[g_1(H_0) + APg_1(H_0/P)] \quad , \\ E &= -[h_1'(H_0) + APh_1'(H_0/P) - 2D\log H_0] \quad , \\ F &= -[h_1(H_0) + AP^2h_1(H_0/P) + 2DH_0(1 - \log H_0) + EH_0] = 0 \quad . \end{aligned} \tag{40}$$

(It can be shown that F is identically zero.) This completes the tip flow solution.

To interpret these results, note that the flow terms $g_1(\eta)$ and $h_1(\eta)$ in (37) represent buoyant rotational flow driven by the lowest order temperature gradient; they decay exponentially in η. The flow terms with coefficient A describe rotational flow (needed to satisfy no-slip at the interface) that decays exponentially in η/P, i.e., this describes the viscous boundary layer. The terms with coefficient D represent a mass sink distributed along the positive z axis whose strength increases linearly with z (as $r \to 0$, $\mathbf{u} \to -(2z/r)\hat{\mathbf{r}} + \log(r^2/4z)\hat{\mathbf{z}}$). The velocity from these terms grows as $\log\eta$, i.e., far away, the dendrite looks like a mass sink, to feed the rising, growing boundary layer. Finally, the flow proportional to E is uniform flow ($\mathbf{u} = \hat{\mathbf{z}}$), which is needed to satisfy no penetration at the interface. So outside the thermal and viscous boundary layers, the perturbation flow becomes irrotational, as expected.

Using this flow solution, we can apply the same approach as above to solve the thermal problem (24), (27), (29), and (30a) for the perturbations to the temperature (T_1) and to the dendrite shape (H_1). Assume solutions of the form

$$\begin{aligned} T_1(\xi,\eta) &= (\xi - 1)\,p(\eta) + q(\eta) \quad , \\ H_1(\xi) &= H_0[(\xi - 1)\,A_0 + A_1] \quad , \end{aligned} \tag{41}$$

where A_0 and A_1 are constants to be determined. Then the problem separates to give

$$(\eta p')' + \eta p' - p = -T_0' g \quad , \tag{42}$$

$$(\eta q')' + \eta q' = -T_0'(g + \frac{1}{2}h) \quad , \tag{43}$$

with the boundary conditions

$$\text{at } \eta = H_0 : \qquad p = -A_0 T_0' \quad , \tag{44}$$

$$q = -A_1 T_0' \quad , \tag{45}$$

$$2A_0 = -S\,[-A_0 H_0 T_0' + p'] \quad , \tag{46}$$

$$A_1 = -S\left[(\frac{1}{2}A_0 - A_1)H_0 T_0' + q'\right] \quad , \tag{47}$$

$$\text{as } \eta \to \infty : \qquad p \to 0 \quad , \qquad q \to 0 \quad , \tag{48}$$

where $g(\eta)$ and $h(\eta)$ are the flow functions defined by (34), each consisting of several terms as shown in (37), and the identity $E_1' + \eta E_1'' = -\eta E_1'$ was used to simplify the boundary conditions.

The general solution can be found by applying variation of parameters for each of the terms in g and h:

$$p(\eta) = \frac{-2}{(1-P)E_1^2(H_0)}\left\{p_1(\eta) + APp_2(\eta) + Dp_3(\eta) + J[E_2(\eta) - E_1(\eta)] + K[\eta + 1]\right\} \quad , \tag{49}$$

$$q(\eta) = \frac{-1}{(1-P)E_1^2(H_0)}\left\{q_1(\eta) + APq_2(\eta) + Dq_3(\eta) + Eq_4(\eta) + LE_1(\eta) + M\right\} \quad . \tag{50}$$

where J, K, L, M are arbitrary constants and

$$p_1(\eta) = \frac{1}{12}\left\{4[E_2(2\eta) - 2E_1(2\eta)] - 3E_1(\eta)[E_2(\eta) - E_1(\eta)] - 2e^{-\eta}[E_2(\eta) - 2E_1(\eta)]\right\} \quad .$$

$$p_2(\eta) = \frac{1}{2}\left\{[E_2(\eta) - E_1(\eta)][2PE_4(\frac{\eta}{P}) - (1+2P)E_3(\frac{\eta}{P}) + 2E_2(\frac{\eta}{P}) - E_1(\frac{\eta}{P})]\right.$$
$$\left. + \frac{1}{P}[\eta + 1][G_{22}(\eta) - G_{21}(\eta) - 2G_{12}(\eta) + 2G_{11}(\eta) + G_{02}(\eta) - G_{01}(\eta)]\right\} \quad ,$$

$$p_3(\eta) = -\left\{[E_2(\eta) - E_1(\eta)][1 - \log\eta] + [\eta + 1]E_1^{(2)}(\eta)\right\} \quad ,$$

$$q_1(\eta) = \frac{1}{2}E_1^2(\eta) + e^{-\eta}E_1(\eta) - 2E_1(2\eta) \quad , \tag{51}$$

$$q_2(\eta) = E_1(\eta)[(1-P)E_3(\frac{\eta}{P}) - (2-P)E_2(\frac{\eta}{P}) + E_1(\frac{\eta}{P})]$$
$$+ \frac{1}{P}[(P-1)G_{21}(\eta) + (2-P)G_{11}(\eta) - G_{01}(\eta)] \quad ,$$

$$q_3(\eta) = 2\left\{E_1(\eta)[1 - \log\eta] + e^{-\eta}(\log\eta - 2) - E_1^{(2)}(\eta)\right\} \quad ,$$

$$q_4(\eta) = -e^{-\eta} \quad .$$

$$\text{and} \quad E_1^{(2)}(\eta) \equiv \int_\eta^\infty \frac{E_1(s)}{s}\, ds \quad ,$$
$$G_{mn}(\eta) \equiv \int_\eta^\infty E_m(\frac{s}{P}) E_n(s)\, ds \quad . \tag{52}$$

Applying the boundary conditions (44-48) determines the constants. For the temperature to decay as $\eta \to \infty$ then $K = M = 0$. Manipulating the boundary conditions to eliminate A_0 and A_1 shows that J and L are determined by

$$H_0 p'(H_0) + (2 + H_0)\, p(H_0) = 0 \quad ,$$
$$H_0 q'(H_0) + (1 + H_0)\, q(H_0) = -p(H_0) \quad . \tag{53}$$

Then the shape perturbation is given by

$$A_0 = S\, p(H_0)/H_0 \quad ,$$
$$A_1 = S\, q(H_0)/H_0 \quad . \tag{54}$$

This completes the solution for the O(G) perturbation. (For one particular Prandtl number $P = 1$ the some of the forms above are undefined, but the limit $P \to 1$ is well defined.)

The complicated form of the solution makes its interpretation difficult. Interpretation can be aided by considering the opposite limits of small or large Peclet number H_0, where asymptotic forms can be used for all the transcendental functions, leading to simpler results at the leading order. While both limits give useful approximate results, the limit of small H_0 is a singular limit, all the different terms becoming unbounded at 0, and the the asymptotic forms are rather complicated.

For large H_0, applying the relations given in the Appendix yields the following asymptotic forms for the main results:

$$A_0 = \frac{1}{4(P+1)H_0} - \frac{17P+7}{8(P+1)^2 {H_0}^2} + \mathrm{O}(\frac{1}{{H_0}^3})$$
$$A_1 = \frac{1}{4(P+1)} - \frac{11P+9}{8(P+1)^2 H_0} + \mathrm{O}(\frac{1}{{H_0}^2}) \tag{55}$$

In this limit, at leading order A_0 decays in H_0 and A_1 approaches a constant (maximum 0.25).

For small H_0, the asymptotic forms are more complicated due to logarithmic singularities at the origin. The results are given as quotients, because inverting the denominators would give an infinite number of terms like $\mathrm{O}(\log^{-n}(H_0))$ before terms of $\mathrm{O}(H_0)$.

$$
\begin{aligned}
A_0 = 2\Bigg\{ & \log(H_0)\left[\frac{2}{3}\log(2) - \frac{P}{2}\mathrm{dilog}(P+1) + \log(P+1)\left(\frac{P^2}{6} - \frac{P}{4} - \frac{1}{2} - \frac{1}{12P}\right)\right. \\
& \left. - \frac{P}{4}\log^2(P) + \log(P)\left(\frac{-P^2}{6} + \frac{P}{4}\right) - \frac{P\pi^2}{12} + \frac{\pi^2}{24} - \frac{P}{6} + \frac{1}{6}\right] \\
& + \left[-\frac{2}{3}\log(2)\log(P) + \frac{2}{3}\log(2)(\gamma+1) - \frac{P}{2}\mathrm{dilog}(P+1)(\gamma+1)\right. \\
& + \log(P+1)(\gamma+1)\left(\frac{P^2}{6} - \frac{P}{4} - \frac{1}{2} - \frac{1}{12P}\right) - \frac{P}{4}\log^2(P)(\gamma+1) \\
& \left. + \log(P)\left((\gamma+1)(-\frac{P^2}{6} + \frac{P}{4}) - \frac{\pi^2}{24} - \frac{1}{12}\right) + (\gamma+1)\left((-2P+1)\frac{\pi^2}{24} - \frac{P-1}{6}\right)\right] + \mathrm{O}(H_0\log^2(H_0))\Bigg\} \Bigg/ \\
& (P-1)\left\{-2\log^3(H_0) + \log^2(H_0)\left[2\log(P) - 6\gamma - 5\right] + \log(H_0)\left[\log(P)(4\gamma+3) - 6\gamma^2 - 10\gamma - 3\right]\right. \\
& \left. + \left[(\log(P) - \gamma - 1)(2\gamma^2 + 3\gamma)\right] + \mathrm{O}(H_0\log^3(H_0))\right\} \qquad (56a)
\end{aligned}
$$

$$
\begin{aligned}
A_1 = \Bigg\{ & \log^2(H_0)\left[-\frac{8}{3}\log(2) + P\mathrm{dilog}(P+1) + \log(P+1)\left(\frac{-2P^2}{3} + \frac{P}{2} + 2 + \frac{5}{6P}\right)\right. \\
& \left. + \frac{P}{2}\log^2(P) + \log(P)\left(\frac{2P^2}{3} - \frac{P}{2}\right) + (2P-1)\frac{\pi^2}{12} + \frac{2}{3}(P-1)\right] \\
& + \log(H_0)\left[\frac{8}{3}\log(2)\log(P) - \frac{2}{3}\log(2)(8\gamma+13) + P\mathrm{dilog}(P+1)(2\gamma+4)\right. \\
& + \log(P+1)\left(\frac{-4P^2\gamma}{3} + P\gamma + 4\gamma + \frac{5\gamma}{3P} - \frac{13P^2}{6} + 2P + \frac{13}{2} + \frac{7}{3P}\right) + P\log^2(P)(\gamma+2) \\
& \left. + \log(P)\left(\frac{\pi^2}{12} + \frac{4P^2\gamma}{3} - P\gamma + \frac{13P^2}{6} - 2P - \frac{1}{6}\right) + (2P-1)(\gamma+2)\frac{\pi^2}{6} + (P-1)\left(\frac{4\gamma}{3} + \frac{13}{6}\right)\right] \\
& + \left[\log(2)\log(P)\left(\frac{8\gamma}{3} + 6\right) + \log(2)\left(\frac{-8\gamma^2}{3} - \frac{26\gamma}{3} - 6\right) + P\mathrm{dilog}(P+1)(\gamma^2 + 4\gamma + 3)\right. \\
& + \log(P+1)\left(\frac{-2P^2\gamma^2}{3} + \frac{P\gamma^2}{2} + 2\gamma^2 + \frac{5\gamma^2}{6P} - \frac{13P^2\gamma}{6} + 2P\gamma + \frac{13\gamma}{2} + \frac{7\gamma}{3F} - \frac{3P^2}{2} + \frac{3P}{2} + \frac{9}{2} + \frac{3}{2P}\right) \\
& + \frac{P}{2}\log^2(P)(\gamma^2 + 4\gamma + 3) \\
& + \log(P)\left(\frac{\pi^2\gamma}{12} + \frac{\pi^2}{4} + \frac{2P^2\gamma^2}{3} - \frac{P\gamma^2}{2} + \frac{13P^2\gamma}{6} - 2P\gamma - \frac{\gamma}{6} + \frac{3P^2}{2} - \frac{3P}{2}\right) \\
& \left. + (2P-1)(\gamma^2 + 4\gamma + 3)\frac{\pi^2}{12} + (P-1)\left(\frac{2\gamma^2}{3} + \frac{13\gamma}{6} + \frac{3}{2}\right)\right] + \mathrm{O}(H_0\log^3(H_0))\Bigg\} \Bigg/ \\
& (P-1)\left\{2\log^4(H_0) + \log^3(H_0)\left[-2\log(P) + 8\gamma + 7\right] + \log^2(H_0)\left[-\log(P)(6\gamma+5) + 12\gamma^2 + 21\gamma + 8\right]\right. \\
& + \log(H_0)\left[-\log(P)(6\gamma^2 + 10\gamma + 3) + 8\gamma^3 + 21\gamma^2 + 16\gamma + 3\right] \\
& \left. + \left[(-\log(P) + \gamma + 1)(2\gamma^3 + 5\gamma^2 + 3\gamma)\right] + \mathrm{O}(H_0\log^4(H_0))\right\} \qquad (56b)
\end{aligned}
$$

where γ is Euler's constant (0.5772...), and the dilogarithm function is defined by

$$\mathrm{dilog}(x) \equiv \int_x^1 \frac{\log(s)}{s-1} ds \quad .$$

following Abramowitz and Stegun (1972). (The lengthy algebraic calculations preceding these results were verified using a symbolic mathematics program called *Mathematica.*)

RESULTS

The above perturbation solution describes in detail the buoyant flow and the resulting thermal field throughout the melt. An example of the buoyant flow is illustrated in Figure 4; in the reference frame of the immobile solid material of the dendrite, this is an instantaneous view of the complete (unsteady) flow as the interface sweeps through. The velocity vectors show the formation of a rising buoyant layer near the dendrite, which satisfies the no-slip condition at the solid surface. In this example ($H_0 = 1$, $P = 2$) the temperature field decays over a dimensionless length scale of about 1; the dropping buoyancy gives a local maximum in the vertical velocity at about that distance. Farther away, the flow is drawn inward to feed the growing buoyant layer. Directly ahead of the dendrite tip there is a weak upward flow, and at (horizontally) farther positions the flow is inward and even downward. In this example, the net effect is that the thermal boundary layer (not shown) is slightly compressed at the tip, leading to enhanced tip growth.

The main results of interest are A_0 and A_1, which describe how buoyancy changes the dendrite's growth Peclet number Pe and shape. The dependence of A_0 and A_1 on the parameters is shown in the next two figures. Figure 5 shows the dependence on the lowest order Peclet number H_0, which is is monotonically related to the Stefan number S (dimensionless undercooling) by the Ivantsov solution (22). The perturbation to the Peclet number is proportional to the *difference* of the two curves:

$$Pe = RV/2\kappa = H|_{\xi=0} = H_0[1 + G(A_1 - A_0)] \quad , \tag{57}$$

where G is the buoyancy parameter. As can be seen, over most of the parameter space (H_0, P), buoyancy increases the Peclet number ($A_1 > A_0$), i.e., growth is enhanced by convection of released latent heat away from the tip. For large undercooling ($H_0 >\sim 1$, $S >\sim 0.6$) the difference $(A_1 - A_0)$ is relatively large, though in practice large S means rapid solidification, so G is small.

It is surprising that there is a range ($P = 0.2$, $H_0 \sim 0.1$) where the curves cross, predicting a very slight *decrease* in the Peclet number from buoyant convection. The interpretation may be that, when viscosity is unimportant ($P \ll 1$) and the dendrite is moderately small, the inward and downward velocities near the tip compress the thermal boundary layer *horizontally* more than the weak vertical velocity directly ahead of the tip compresses it *vertically.* Then the net effect would be a smaller thermal gradient and slower growth, at the tip.

The departure of the shape of the dendrite from a paraboloid depends only on A_0. If it were a paraboloid, then the dimensionless interface position $H(\xi)$ would be constant, so the departure is $H(\xi) - H_0(1 + GA_1) = GH_0A_0(\xi - 1)$. The fact that A_0 is positive means

that the tip ($\xi < 1$) is relatively smaller, but the dendrite widens further down ($\xi > 1$) , because the buoyant flow redistributes the heat away from the tip towards the base of the dendrite.

Comparing Figures 5a, 5b, and 5c shows that the Prandtl number P has a large effect on the magnitudes of A_0 and A_1, as well as some effect on their H_0-dependence. Figure 6 shows the dependence on Prandtl number P, for $H_0 = 1$, i.e., $S = 0.596$. It can be seen that when P is large, buoyant effects are relatively small. This makes sense, in that the high viscosity inhibits flow in the thermal layer, near the no-slip interface, so little heat is convected. At the other extreme, the results become nearly independent of P, because the viscous layer near the interface is much thinner than the thermal layer, so the buoyant flow is limited primarily by inertia.

The asymptotic approximations of the solution for large and small H_0 are compared with the actual solution (for $P = 2$) in Figure 7. (At each extreme, both the leading-order approximation and the next higher-order approximation are shown.) It is apparent that the asymptotic forms converge well, so are useful in those limits. This is fortunate, because the actual solution becomes difficult to calculate at both extremes, due to exponential dependence for large H_0 and due to logarithmic singularities for small H_0.

To see how the Ivantsov solution is modified by buoyancy, Figure 8 shows growth speed V versus tip radius R, holding constant the physical parameters, i.e., undercooling, material properties, and gravity. This represents the family of possible physical solutions corresponding to one particular dimensionless solution. (The lack of a unique physical solution comes from neglecting surface energy in the problem statement.) Then the form of the relation of R and V is

$$R = \frac{A}{V} + \frac{B}{V^4} \quad , \tag{58}$$

where $A = 2\kappa H_0$ and $B = 2g\alpha(T_m - T_\infty)\kappa^2 H_0(A_1 - A_0)$. For the Ivantsov solution, $B = 0$, giving a straight line on the logarithmic plot, and for large V the buoyant solution is close to this line. But for slow growth (small V, large buoyant parameter G) the buoyant solution departs from the Ivantsov solution, giving relatively faster growth for a given tip radius (or a smaller tip for a given speed).

Choosing one member of this family of solutions requires some selection criterion outside the scope of this paper. One criterion that seems to match experimental data well (Huang and Glicksman, 1981a) comes from considering the morphological stability of the dendrite tip; the criterion is of the form

$$\frac{2\kappa d_0}{VR^2} = \sigma \quad \text{(constant)} \quad , \tag{59}$$

where κ is the thermal diffusivity, $d_0 \equiv T_m \gamma C_p / L^2$ is a capillary length, T_m is the melting temperature, γ is the surface energy, C_p the volumetric specific heat, and L the volumetric latent heat of fusion. Different theories give different values for the constant σ, but the value determined experimentally by Huang and Glicksman (1981a) for succinonitrile is $\sigma = 0.0195$. This selection criterion is also shown on Figure 8; following this criterion shows that buoyant convection gives both faster growth and a smaller tip radius, relative to the non-buoyant (Ivantsov) case.

The predictions of the buoyant theory, augmented by the selection criterion $\sigma = 0.0195$, are compared to the experiments of Huang and Glicksman (1981a) on succinonitrile in Figure 9. The values used for the physical constants are: $\kappa = 1.16 \times 10^{-3}\text{cm}^2/\text{s}$, $P = 22.8$, $L = 885.1\text{cal/mole}$, $C_p = 38.25\text{cal/mole K}$, $\alpha = 5.0 \times 10^{-4}\text{K}^{-1}$, $d_0 = 2.7 \times 10^{-7}\text{cm}$, and $g = 980\text{cm/s}^2$ (from Huang and Glicksman, 1981b and 1981a).

At high Stefan number S (undercooling), buoyant convection is slow compared to the interface motion (the buoyancy parameter G is small), and so buoyant effects are negligible. As the Stefan number decreases, the growth speed V also decreases, and the buoyant parameter G becomes significant. Both theory and experiments show that, relative to the non-buoyant case, buoyant convection increases the growth Peclet number Pe, enhances the speed V of growth, and decreases the radius R of the dendrite tip. However, for very small undercooling, the theoretical predictions fail to match the experiments, overpredicting convective effects, due to neglecting the nonlinear inertial terms. Nonetheless, considering that the buoyant perturbation solution is based on the assumption that the buoyancy parameter is small ($G \ll 1$), the range of agreement is surprisingly good (up to $G \sim 5000$).

CONCLUSIONS

Because of the importance of solidification in the processing of materials, a theoretical understanding of the details of solidification is of practical interest. Currently, processing materials in a microgravity environment is possible, but very expensive, so prediction of gravitational effects in solidification may be helpful in deciding when the expense is justified.

The present work considers one special case: buoyant convection effects on an isolated dendrite of a pure substance, solidifying downward into an undercooled melt. To further simplify the problem, it is assumed that the dendrite is smooth and axisymmetric, that surface energy effects are negligible, and that buoyant velocities are small relative to the speed of the solidification interface. The dimensionless problem depends on three parameters: Stefan number $S = (T_m - T_\infty)C_p/L$ (undercooling), Prandtl number P, and buoyancy parameter $G = g\alpha(T_m - T_\infty)\kappa/V^3$, where $G \ll 1$ by the last assumption above.

The buoyancy parameter G is the product of a Rayleigh number and the Prandtl number P. For small P, inertia limits the flow and G gives a dimensionless measure of the importance of buoyant convection. However, for large Prandtl number, viscosity limits the flow, and a better measure of the importance of buoyancy is the Rayleigh number, G/P. One measure that covers both cases is $G/(P+1)$.

The solution is constructed as a regular perturbation in G about the non-buoyant paraboloidal solution due to Ivantsov (1947). The first-order ($O(G^1)$) perturbation quantities describing the buoyant flow and temperature throughout the melt, and the perturbed interface position, are given in closed form above, showing explicitly the dependence on S and P. The perturbation solution is not uniformly valid in space; it applies within a dimensionless distance of $O(G^{-1}) \gg 1$ from the dendrite tip.

The main result of interest is the dimensionless position of the solid-liquid interface in axisymmetric parabolic coordinates (ξ, η):

$$\text{interface at: } \eta = H(\xi; S, P, G) = H_0(S)\left\{1 + G[(\xi - 1)A_0(S, P) + A_1(S, P)]\right\} \quad , \quad (60)$$

where H_0 is the Ivantsov solution, given by (22), the buoyant perturbations A_0 and A_1 are given by (54), and Figures 5 and 6 show that $A_1 > A_0 > 0$ (with the exception discussed in the Results section).

This result predicts two main effects of buoyant convection: enhanced growth and a modified shape. At the very tip of the dendrite, $\xi = 0$, and the dimensionless radius of curvature is 2η, so the growth Peclet number is

$$Pe \equiv \frac{RV}{2\kappa} = H|_{\xi=0} = H_0[1 + G(A_1 - A_0)] \quad , \tag{61}$$

where R and V are the dimensional tip radius and growth speed. Thus, because G and $(A_1 - A_0)$ are positive, buoyancy enhances growth for a downward-growing dendrite. (Figure 5c shows the exception: for small P and a narrow range of H_0, the difference $A_1 - A_0$ is slightly negative, predicting slightly reduced growth at the tip, presumably from convection inward and downward nearby.)

The dependence of the dimensionless interface position H on ξ in (60) shows that the dendrite is not a paraboloid; because $A_0 > 0$, the tip is smaller, and toward the root the dendrite widens, relative to a paraboloid. This buoyant modification of the dendrite shape is a unique feature of the current work; previous analyses assume a paraboloid shape. Furthermore, while the dimensionless solution cannot predict R and V separately, the use of any selection criterion of the form R^2V = constant (such as criteria based on tip stability) will predict both faster growth and a smaller tip due to buoyant convection of released latent heat away from the tip, toward the root.

The magnitude of these buoyant effects depends strongly on the Prandtl number of the melt, as shown in Figure 6. For large P, the viscous length scale is larger than the thermal layer, and the no-slip solid interface inhibits convection, so buoyant effects are relatively small. However, for small P, the viscous layer by the interface is thin relative to the thermal layer, so the buoyant convection is effectively inviscid, limited by inertia, and buoyant effects are relatively large. Thus, conclusions based on experiments or calculations for a high-Prandtl number material (e.g., succinonitrile: $P = 23$) should be applied cautiously to the processing of low-Prandtl number materials (e.g., metals), and vice versa.

Due to the neglect of nonlinear inertial terms, the present work overpredicts buoyant effects when G is large. However, the theory (with the selection criterion based on stability) matches the experiments well up to $G \sim 5000$, despite the formal assumption that $G \ll 1$. In comparison, the nonlinear calculations of Ananth and Gill (1988) match the experiments well even for large G; their selection criterion involves choosing the Grashof number to fit the experimental Peclet number. Their method, which assumes the dendrite is a paraboloid, requires numerically solving a pair of coupled nonlinear ordinary differential equations for each set of parameters, and their published results are limited to one Prandtl number ($P = 23.1$). The results of the present work are expressed in closed form, and are relatively easy to calculate, involving only a few different transcendental functions and several arithmetic combinations. (Rough predictions can be made by interpolation using Figures 5 and 6.)

While the perturbation solution applies only for a downward growing dendrite, the perturbations (by assumption) are linear in the buoyancy parameter G, and it is tempting

to apply the same solution to an upward growing dendrite by merely reversing the sign of G. We speculate that this may give reasonable results if the magnitude of G is small enough, so that the speed of the interface as it sweeps through, freezing the material, overwhelms the instantaneous local fluid velocity. However, for larger buoyancy, i.e., slow solidification, the thermal layer of fluid rising toward the tip of the dendrite could keep rising past the tip, forming a plume above the dendrite. Such a plume would change the character of the flow completely, so the perturbation solution would not apply.

The buoyant perturbation solution can also be interpreted to apply to the growth of a dendrite of a binary alloy, if the process is controlled by the mass diffusion of solute rejected at the solidification front (as discussed in the Problem Statement). This would be the case if the mass diffusivity D of the solute is much smaller than the thermal diffusivity κ in the melt, and if the latent heat is negligible. Then the temperature is effectively constant (T_∞), and the transport problem reduces to convection and diffusion of solute, measured by its concentration C. To interpret the solution for this alloy problem, substitute C for T, nondimensionalize using D instead of κ, and the new dimensionless parameters become $S \to (C_l - C_\infty)/(C_l - C_s)$, $P \to Sc \equiv \nu/D$, and $G \to g\beta(C_l - C_\infty)D/V^3$, where C_s is the concentration in the solid, C_l in the liquid at the interface, and C_∞ deep into the melt, Sc is the Schmidt number, and β is a solutal coefficient of expansion, defined by $(\rho - \rho_\infty)/\rho_\infty = \beta(C - C_\infty)$.

The methods employed here may also apply to dendrites shaped more like elliptic paraboloids. The key element that makes the perturbation analysis feasible here is the existence of a simple solution to the nonbuoyant case, depending only on one coordinate in a separable coordinate system, that gives the shape of the free boundary and accounts for the nonlinear flux condition at the interface. The family of such solutions is quite extensive (Canright and Davis, 1989), including one for an elliptic paraboloid. (In fact, solutions are known for binary alloys when both thermal and solutal variations are important, or ternary alloys when thermal variations are negligible, so the perturbation approach may be applicable to such cases as well.) The detailed form of a buoyant perturbation to the elliptic-paraboloid basic state would be more complicated than the solution given here, in that the flow would depend on all three spatial coordinates, and the special functions may also be more complicated. We speculate that the qualitative features in that case may be similar to those of the present case.

ACKNOWLEDGEMENTS

This work was supported in part by a grant from the National Aeronautics and Space Administration, Microgravity Science and Applications Program, and in part by the Naval Postgraduate School Research Council. The authors are grateful to Dr. S.C. Huang for providing the experimental data cited, in tabular form.

APPENDIX: SPECIAL FUNCTIONS IN SOLUTION

In the perturbation solution, the various functions (g's, h's, p's, q's) describing the stream function and temperature perturbations are expressed in terms of exponential integrals E_n and integrals thereof.

The exponential integrals are standard functions, and can be found in standard references, e.g., Abramowitz and Stegun (1972). Some of their properties are recounted here, for convenience. The definition is

$$E_n(x) \equiv \int_1^\infty \frac{e^{-xs}}{s^n} ds \quad , \tag{62}$$

where we are only concerned with non-negative integer values for n. Some special cases are

$$E_0(x) = \frac{e^{-x}}{x} \quad , \qquad E_1(x) = \int_x^\infty \frac{e^{-s}}{s} ds \quad . \tag{63}$$

Differentiating the definition shows that the derivatives are

$$\frac{d}{dx} E_n(x) = -E_{n-1}(x) \quad . \tag{64}$$

Integrating the definition by parts gives

$$E_{n+1}(x) = \frac{1}{n} \left[e^{-x} - x E_n(x) \right] \quad . \tag{65}$$

This can be used to reduce all such exponential integrals E_n to forms involving only the special function E_1. At the origin, E_1 has a logarithmic singularity

$$E_1(x) = -(\log x + \gamma) - \sum_{k=1}^{\infty} \frac{(-x)^k}{k k!} \quad , \tag{66}$$

where $\gamma \approx 0.5772$ is Euler's constant. For large arguments, the asymptotic series is

$$E_1(x) \sim \frac{e^{-x}}{x} \sum_{k=0}^{\infty} \frac{k!}{(-x)^k} \quad . \tag{67}$$

The function $E_1^{(2)}$ is less common, but has applications to stellar atmospheres. It was first defined by van de Hulst (1948); we use his notation:

$$E_1^{(2)}(x) \equiv \int_x^\infty \frac{E_1(s)}{s} ds \quad . \tag{68}$$

Switching the order of integration, this can also be expressed as

$$E_1^{(2)}(x) = \int_1^\infty \frac{e^{-xs} \log s}{s} ds. \quad , \tag{69}$$

which is more convenient for numerical calculation. (Kourganoff, 1952, Appendix I) shows this result and many others related to exponential integrals.) Near the origin, the following expansion, due to van de Hulst (1948), converges quickly:

$$E_1^{(2)}(x) = \frac{1}{2}(\log x + \gamma)^2 + \frac{\pi^2}{12} + \sum_{k=1}^{\infty} \frac{(-x)^k}{k^2 k!} \quad . \tag{70}$$

For large arguments, integration by parts gives the following asymptotic series:

$$E_1^{(2)}(x) \sim \frac{e^{-x}}{x} \sum_{k=1}^{\infty} \left[\frac{(-1)^{k-1} k!}{x^k} \sum_{j=1}^{k} \frac{1}{j} \right] \quad . \tag{71}$$

(We have not seen this or subsequent results published previously.)

Van de Hulst (1948) defined certain functions he called G_{mn}; the functions we call G_{mn} are similar to, but different from, his functions. We use the definition

$$G_{mn}(x) \equiv \int_x^{\infty} E_m(\frac{s}{P}) E_n(s)\, ds \quad , \tag{72}$$

where the parameter P is the Prandtl number for our purposes. Following the methods used by Chandrasekhar (1950, Appendix I), i.e., integration by parts and the identities for E_n, all of the G_{mn} we need can be reduced to simpler functions:

$$\begin{aligned}
G_{02}(x) &= -P^2 e^{-x/P} E_1(x) + (P + P^2) E_1(\beta x) \quad , \\
G_{11}(x) &= e^{-x} E_1(x/P) + P e^{-x/P} E_1(x) - x E_1(x) E_1(x/P) - (P+1) F_1(\beta x) \quad , \\
G_{12}(x) &= \frac{1}{2} \Big[P e^{-\beta x} + (1-x) e^{-x} E_1(x/P) - (P^2 + Px) e^{-x/P} E_1(x) \\
&\quad + x^2 E_1(x) E_1(x/P) + (P^2 - 1) E_1(\beta x) \Big] \quad , \\
G_{21}(x) &= \frac{1}{2} \Big[e^{-\beta x} - \frac{1}{P}(1+x) e^{-x} E_1(x/P) + (P - x) e^{-x/P} E_1(x) \\
&\quad + \frac{x^2}{P} E_1(x) E_1(x/P) - (P - \frac{1}{P}) E_1(\beta x) \Big] \quad , \\
G_{22}(x) &= \frac{1}{3} \Big[(P + 1 - x) e^{-\beta x} - \frac{1}{P}(1 + x - x^2) e^{-x} E_1(x/P) - \\
&\quad - (P^2 + Px - x^2) e^{-x/P} E_1(x) - \frac{x^3}{P} E_1(x) E_1(x/P) + (P^2 + \frac{1}{P}) E_1(\beta x) \Big] \quad ,
\end{aligned} \tag{73}$$

where $\beta \equiv 1 + \frac{1}{P}$. The one exception is G_{01}, which apparently cannot be reduced to standard functions. By definition,

$$\frac{1}{P} G_{01}(x) = \int_x^{\infty} \frac{e^{-s/P}}{s} E_1(s) ds \quad . \tag{74}$$

Switching the order of integration yields a form more amenable to numerical computation:

$$\frac{1}{P} G_{01}(x) = \int_{\beta x}^{\infty} \frac{e^{-s}}{s} \log\left(\frac{s}{x} - \frac{1}{P} \right) ds \quad . \tag{75}$$

Near the origin, the series representation is

$$\begin{aligned}\frac{1}{P}G_{01}(x) &= \frac{1}{2}(\log x+\gamma)^2 - \frac{\pi^2}{12} - \log^2 P - \mathrm{dilog}(P+1) \\ &+ (-(\log x+\gamma) - P + 1)\frac{x}{P} + ((\log x+\gamma) + \frac{1}{2}(P^2+4P-1))\frac{x^2}{4P^2} \\ &+ (-(\log x+\gamma) - \frac{1}{6}(2P^3+9P^2+18P-1))\frac{x^3}{18P^3} + \mathrm{O}(x^4\log x) \quad ,\end{aligned} \tag{76}$$

where the dilogarithm function is defined by $\mathrm{dilog}(t) \equiv -\int_1^x \frac{\log s}{s-1} ds$, following Abramowitz and Stegun (1972). (The general form for the n^{th} term is not apparent.) Integration by parts gives the asymptotic series for large arguments:

$$\frac{1}{P}G_{01}(x) \sim \frac{Pe^{-\beta x}}{x}\sum_{k=1}^{\infty}\left[\frac{(-1)^{k-1}k!}{x^k}\sum_{j=1}^{k}\frac{1}{j\beta^{k-j+1}}\right] \quad . \tag{77}$$

Using the reductions above, all the perturbation functions (g's, h's, p's, q's) can be expressed in forms where the only special functions are E_1, $E_1^{(2)}$, and G_{01}:

$$\begin{aligned}
g_1(x) &= \frac{1}{2}\left[(1+x)e^{-x} - (2x+x^2)E_1(x)\right] \quad , \\
h_1(x) &= -xe^{-x} + (x+x^2)E_1(x) \quad , \\
p_1(x) &= \frac{1}{12}\left\{2e^{-2x} + (1+2x)e^{-x}E_1(x) + (1+x)\left[3E_1^2(x) - 8E_1(2x)\right]\right\} \quad , \\
p_2(x) &= \frac{1}{12}\left\{-\frac{2P^2-5P+1}{P}e^{-\beta x} + (\frac{-6P^2+6P+1}{P^2} + \frac{2}{P^2}x)e^{-x}E_1(x/P)\right. \\
&\quad \left. + (1+x)\left[6\left(E_1(x)E_1(x/P) - \frac{1}{P}G_{01}(x)\right) + \frac{2P^3-3P^2-6P-1}{P^2}E_1(\beta x)\right]\right\} \quad , \\
p_3(x) &= (\log x - 1)e^{-x} - (1+x)\left[(\log x-1)E_1(x) + E_1^{(2)}(x)\right] \quad , \\
q_1(x) &= \frac{1}{2}\left\{2e^{-x}E_1(x) + \left[E_1^2(x) - 4E_1(2x)\right]\right\} \quad , \\
q_2(x) &= \frac{1}{2}\left\{\frac{P-1}{P}e^{-\beta x} + (\frac{-2P^2+3P+1}{P^2} - \frac{P-1}{P^2}x)e^{-x}E_1(x/P)\right. \\
&\quad \left. + \left[2\left(E_1(x)E_1(x/P) - \frac{1}{P}G_{01}(x)\right) + \frac{P^3-P^2-3P-1}{P^2}E_1(\beta x)\right]\right\} \quad , \\
q_3(x) &= 2\left\{(\log x-2)e^{-x} - \left[(\log x-1)E_1(x) + E_1^{(2)}(x)\right]\right\} \quad .
\end{aligned} \tag{78}$$

To calculate these functions, standard mathematical software libraries have built-in functions for the exponential integral and routines for evaluating the integrals (69) and (75) defining $E_1^{(2)}$ and G_{01}. For extreme values of the arguments, the appropriate series for $E_1^{(2)}$ and G_{01} may be more accurate than numerical integration.

REFERENCES

Abramowitz, M. & Stegun, I. A. 1972 *Handbook of Mathematical Functions.* Dover Publications.

Ananth, R. & Gill, W. N. 1988 Dendritic growth with thermal convection. *J. Crystal Growth* **91**, 587-598.

Canright, D. & Davis, S.H. 1989 Similarity solutions for phase-change problems. *Metallurgical Transactions* **20A**, 225-235.

Chandrasekhar, S. 1950 *Radiative transfer.* Oxford University Press.

Huang, S.-C. & Glicksman, M. E. 1981a Fundamentals of dendritic solidification - I: Steady-state tip growth. *Acta Metall.* **29**, 701- 715.

Huang, S.-C. & Glicksman, M. E. 1981b The influence of natural convection on dendritic growth. Technical Report 81CRD287, General Electric Company, Corporate Research and Development.

Ivantsov, G.P. 1947 *Doklady Akademii Nauk, SSSR.* **58**, 567-569.

Kourganoff, V. 1952 *Basic methods in transfer problems.* Oxford University Press.

Tirmizi, S.H. & Gill, W.N. 1987 Effect of natural convection on growth velocity and morphology of dendritic ice crystals. *Journal of Crystal Growth* **85**, 488-502.

van de Hulst, H.C. 1948 Scattering in a planetary atmosphere. *Astrophysical Journal* **107**, 220-246.

FIGURE CAPTIONS

Figure 1. Problem schematic: Relative to the growing dendrite surface, the liquid moves steadily up and through the interface as it becomes solid. Axisymmetry is assumed; gravity is downward. Far from the dendrite the liquid is undercooled and in uniform motion.

Figure 2. Parabolic coordinates: Lines of constant η (solid) and ξ (dashed) are shown; equal steps in η and ξ correspond to equal distances along the z-axis.

Figure 3. Regions of flow: The perturbation solution applies within a distance $O(G^{-1})$ from the dendrite tip. In the buoyant layer further downstream convection is nonlinear. In the far field the flow is irrotational but not of separable form.

Figure 4. Buoyant flow: an example of the instantaneous flow field (velocity vectors) near the dendrite tip, relative to the solid material (the interface moves downward at speed V): $H_0 = 1$ ($S = 0.6$), $P = 2$.

Figure 5. Interface perturbations A_0 (solid) and A_1 (dashed) as functions of H_0: (a) $P = 20$; (b) $P = 2$; (c) $P = 0.2$.

Figure 6. Interface perturbations A_0 (solid) and A_1 (dashed) as functions of P, for $H_0 = 1$.

Figure 7. Asymptotic approximations: For $P = 2$, A_0 (7a) and A_1 (7b) are shown (solid), with small-H_0 asymptotic forms to O(1) (as in Eq. 56) (dashed) and to $O(H_0)$ (dotted), and large-H_0 asymptotic forms using one term (dashed) and two terms (see Eq. 55) (dotted).

Figure 8. Comparison with Ivantsov solution: For one dimensionless solution ($S = 0.02$, $H_0 = 0.004$, $P = 22.8$) the relation between growth speed V (cm/s) and tip radius R (cm) is shown, using material constants for succinonitrile: perturbation theory (solid), and Ivantsov solution (dashed). The selection criterion $\sigma = 0.0195$ is also shown (dotted).

Figure 9. Comparison with experiments: Both perturbation theory (solid) and the Ivantsov solution (dashed) (both using the selection criterion $\sigma = 0.0195$) are shown with experimental data points (dots) from Huang and Glicksman (1981): (a) Peclet number Pe versus Stefan number S; (b) growth speed V (cm/s) versus Stefan number S; (c) tip radius R (cm) versus Stefan number S; (d) buoyancy parameter G versus Stefan number S.

Figure 1

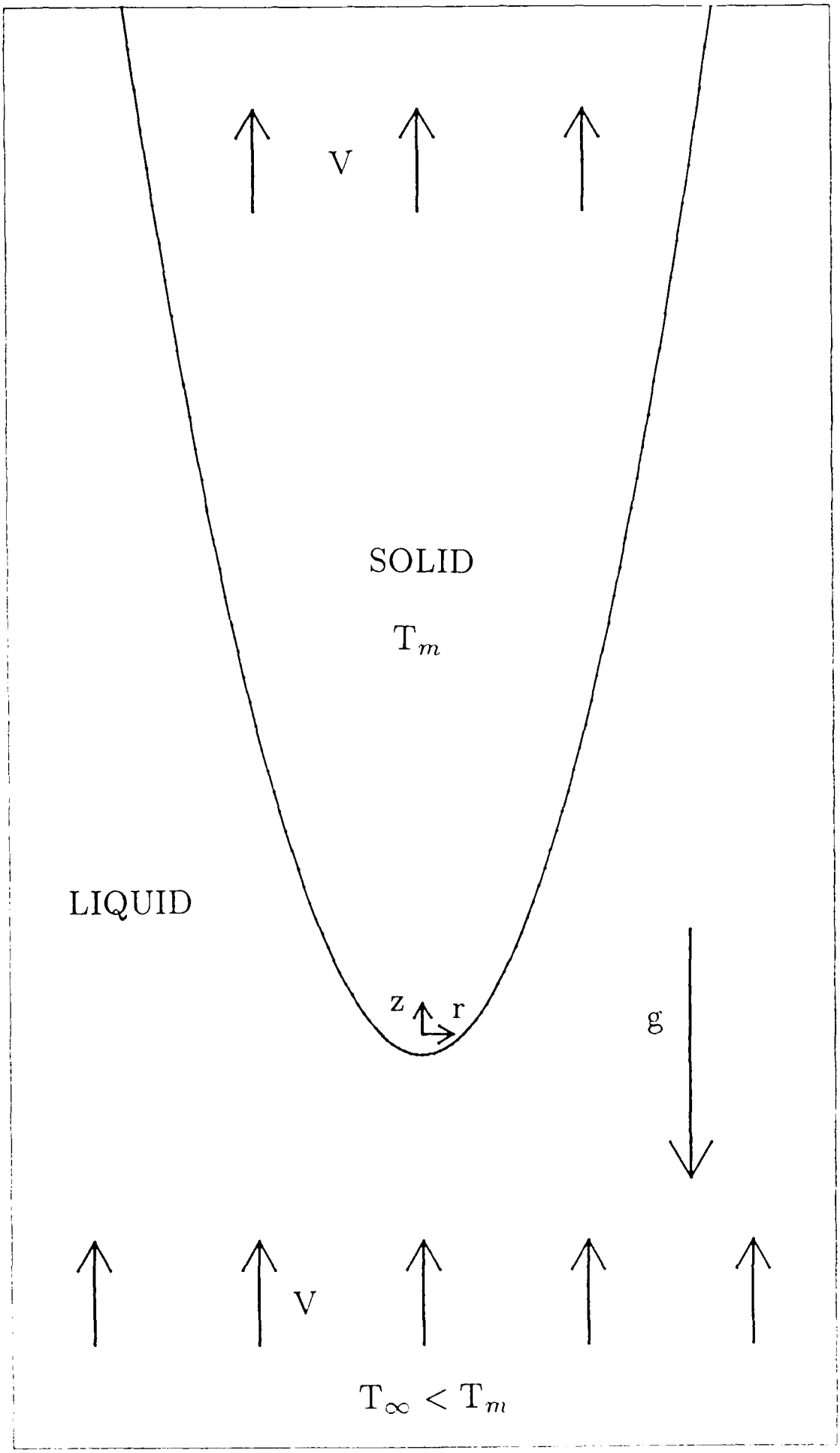

Figure 2

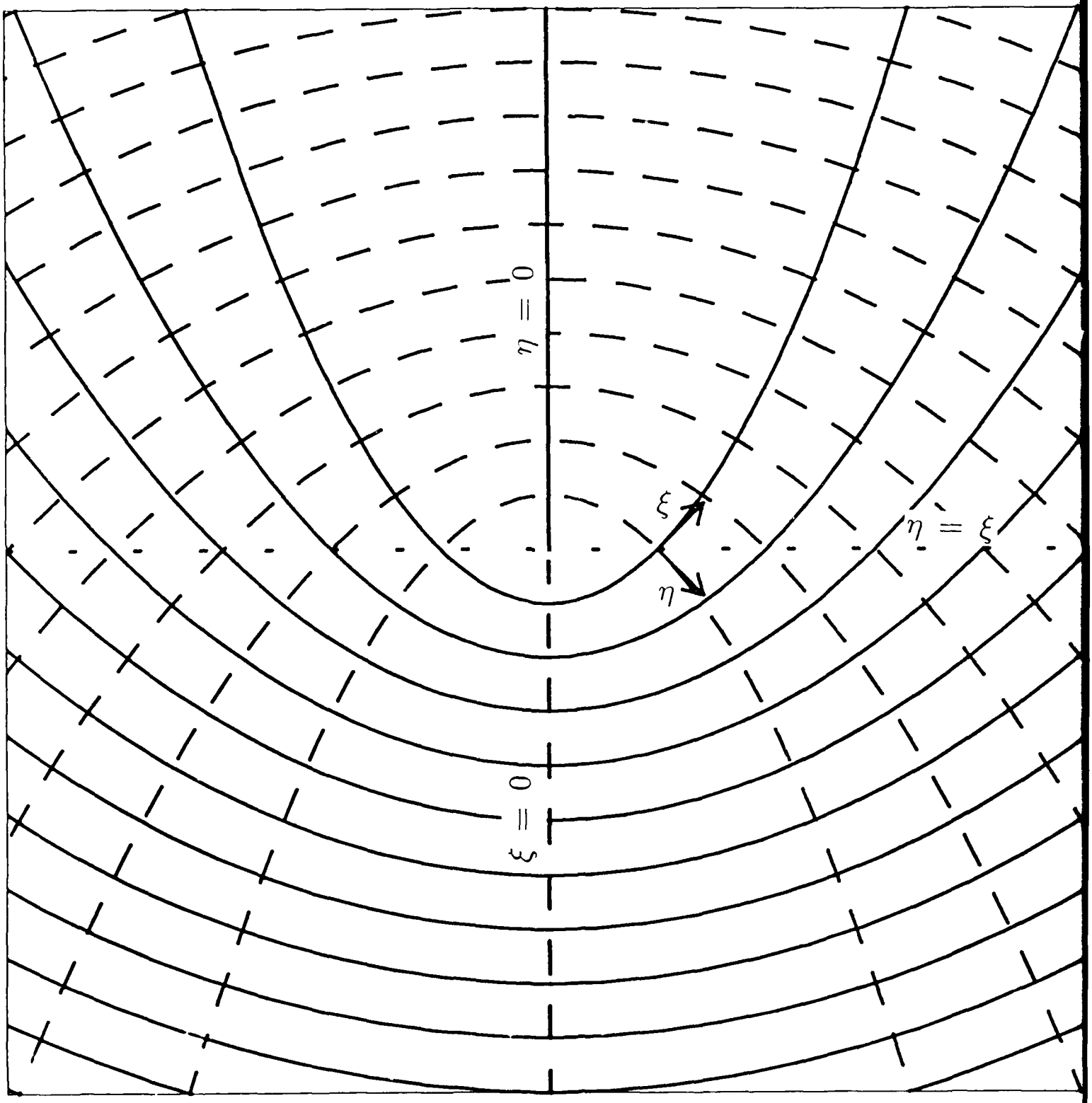

Figure 3

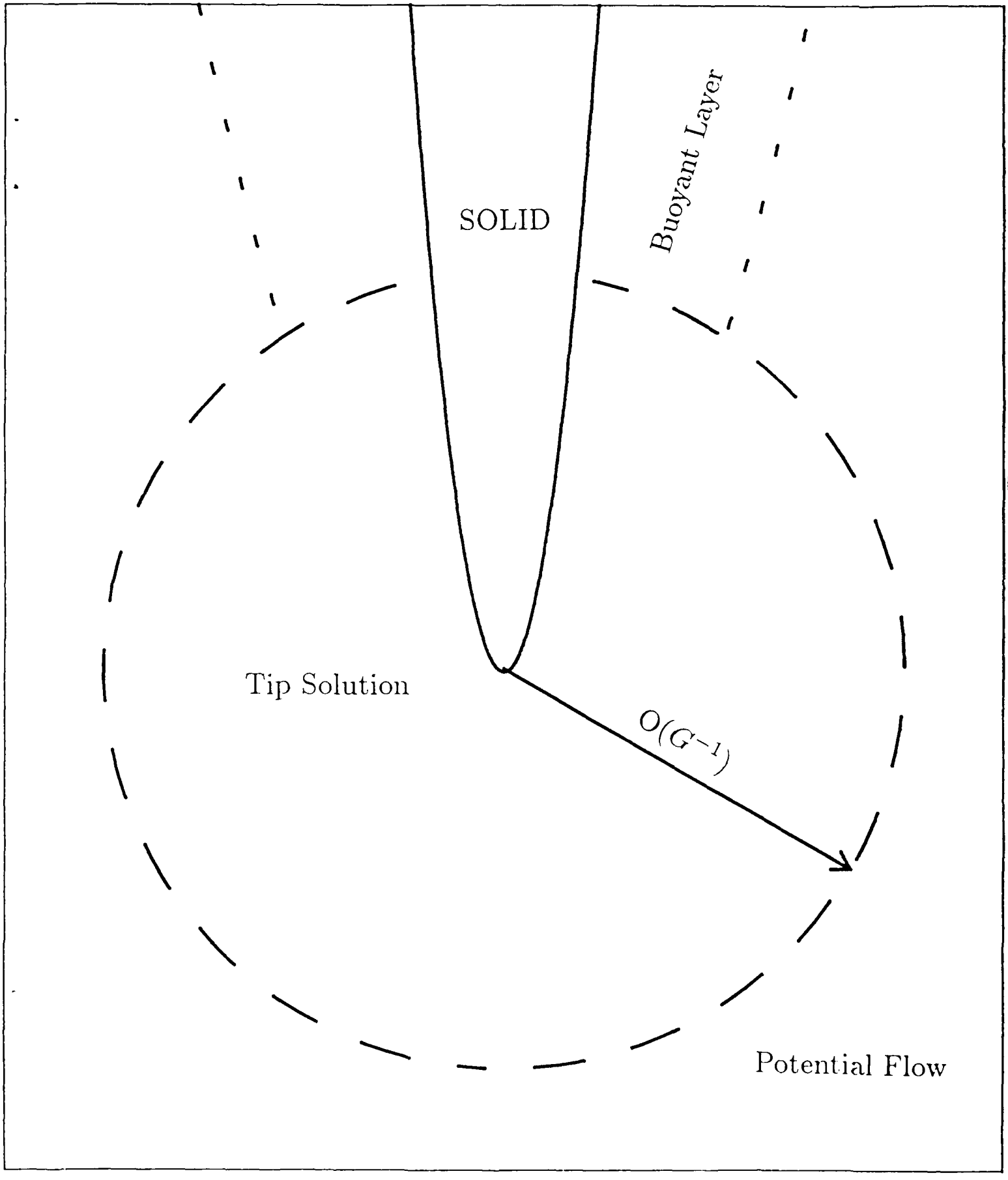

Figure 4

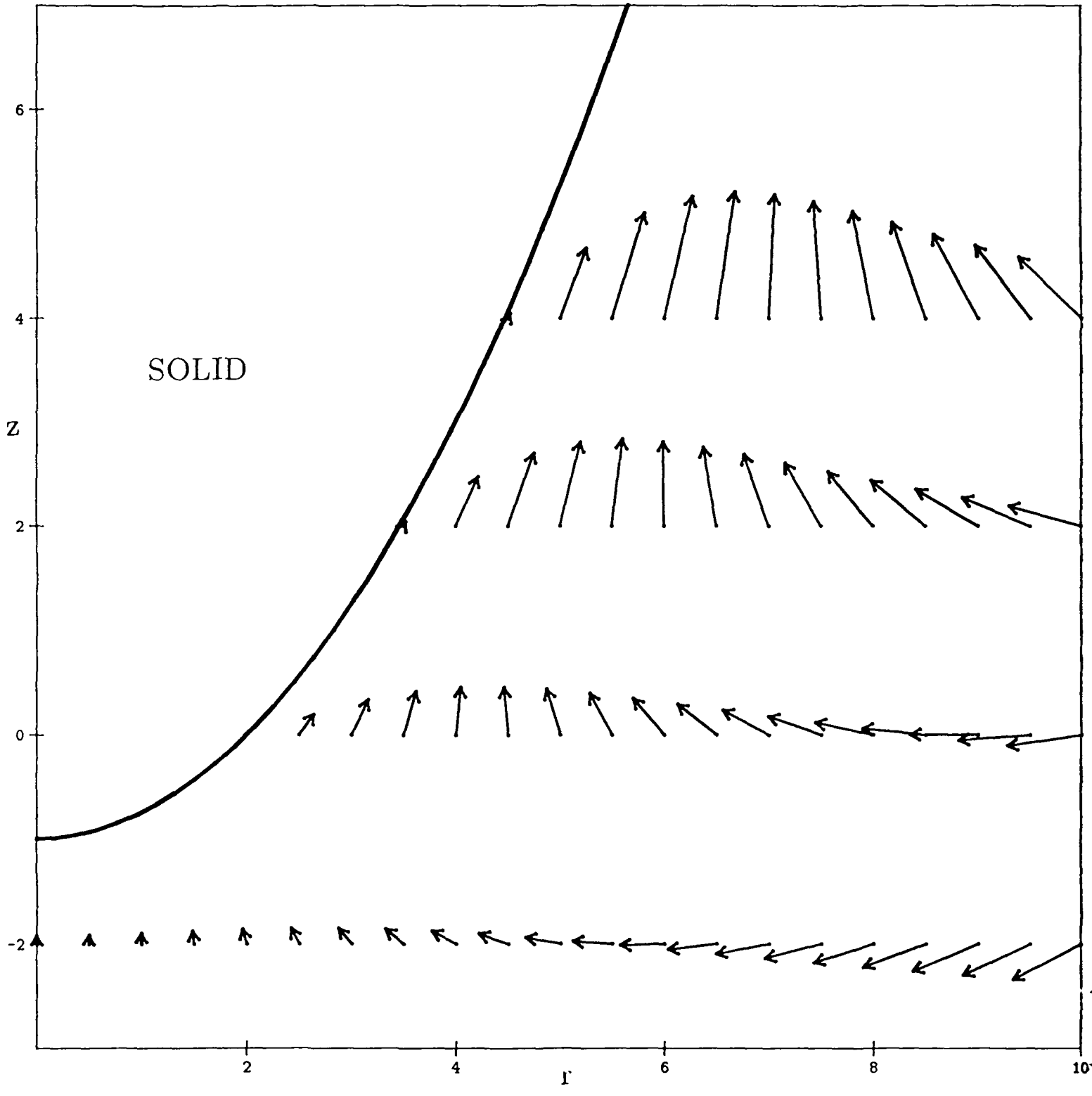

Figure 5a

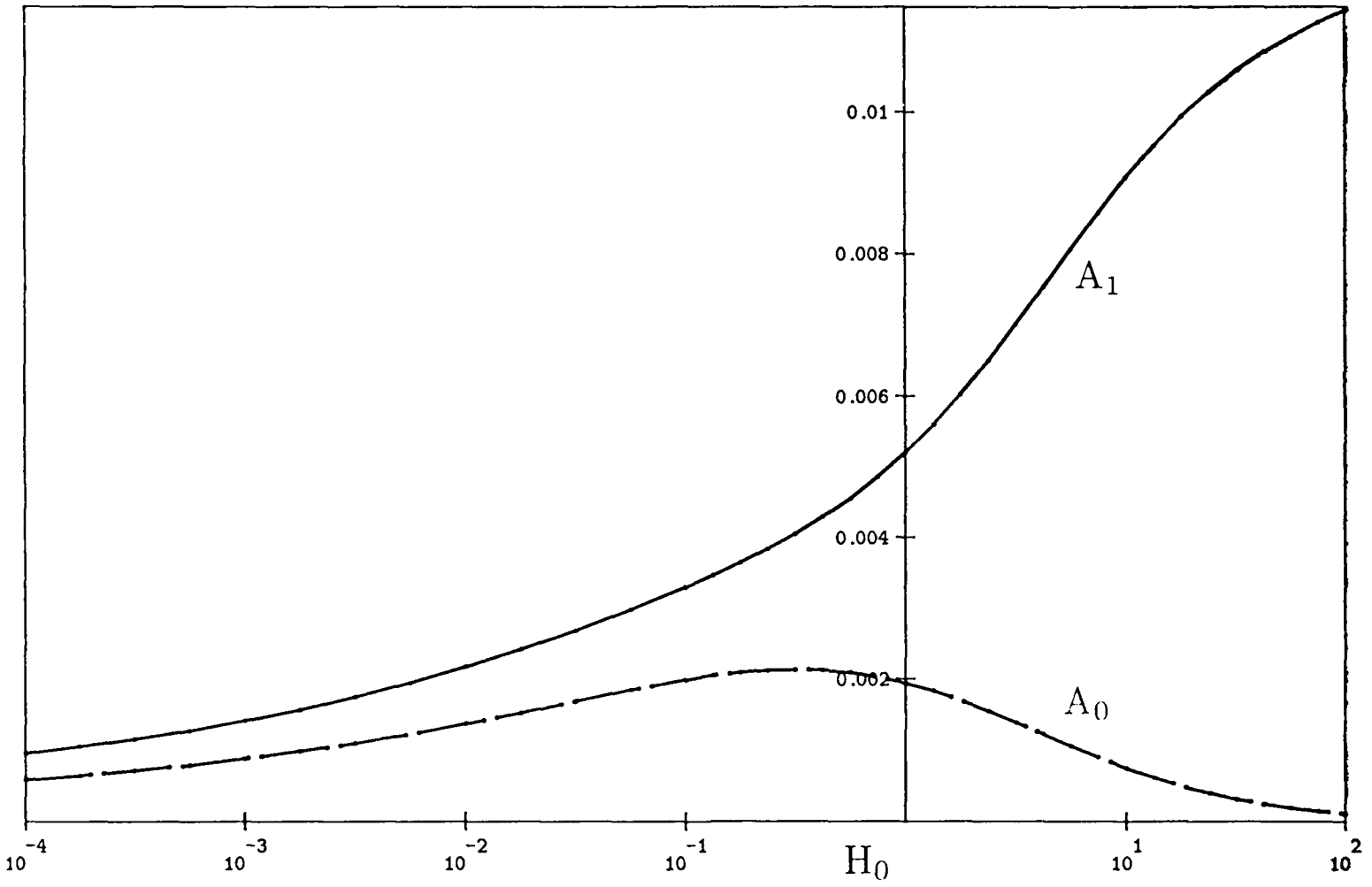

Figure 5b

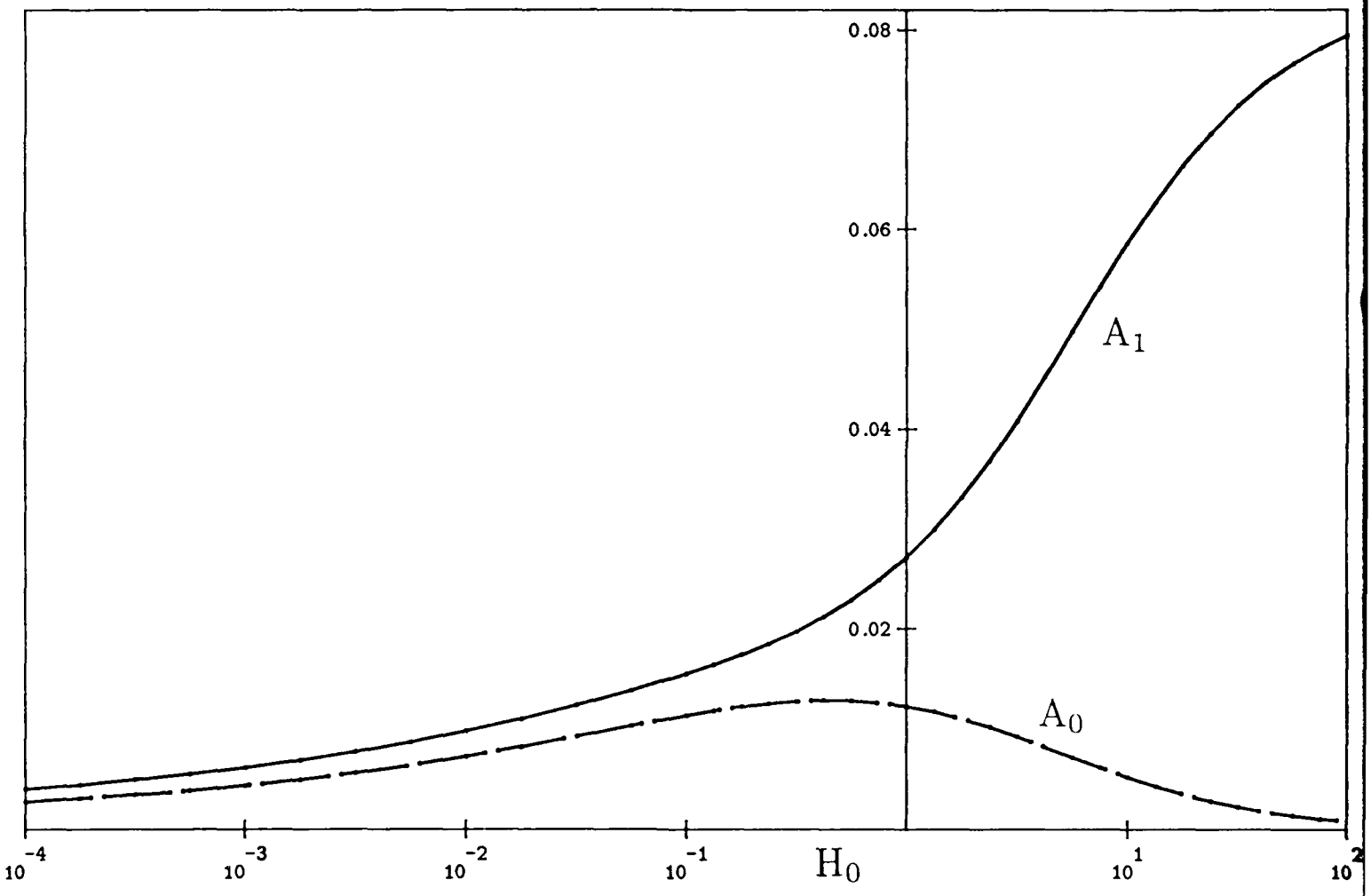

Figure 5c

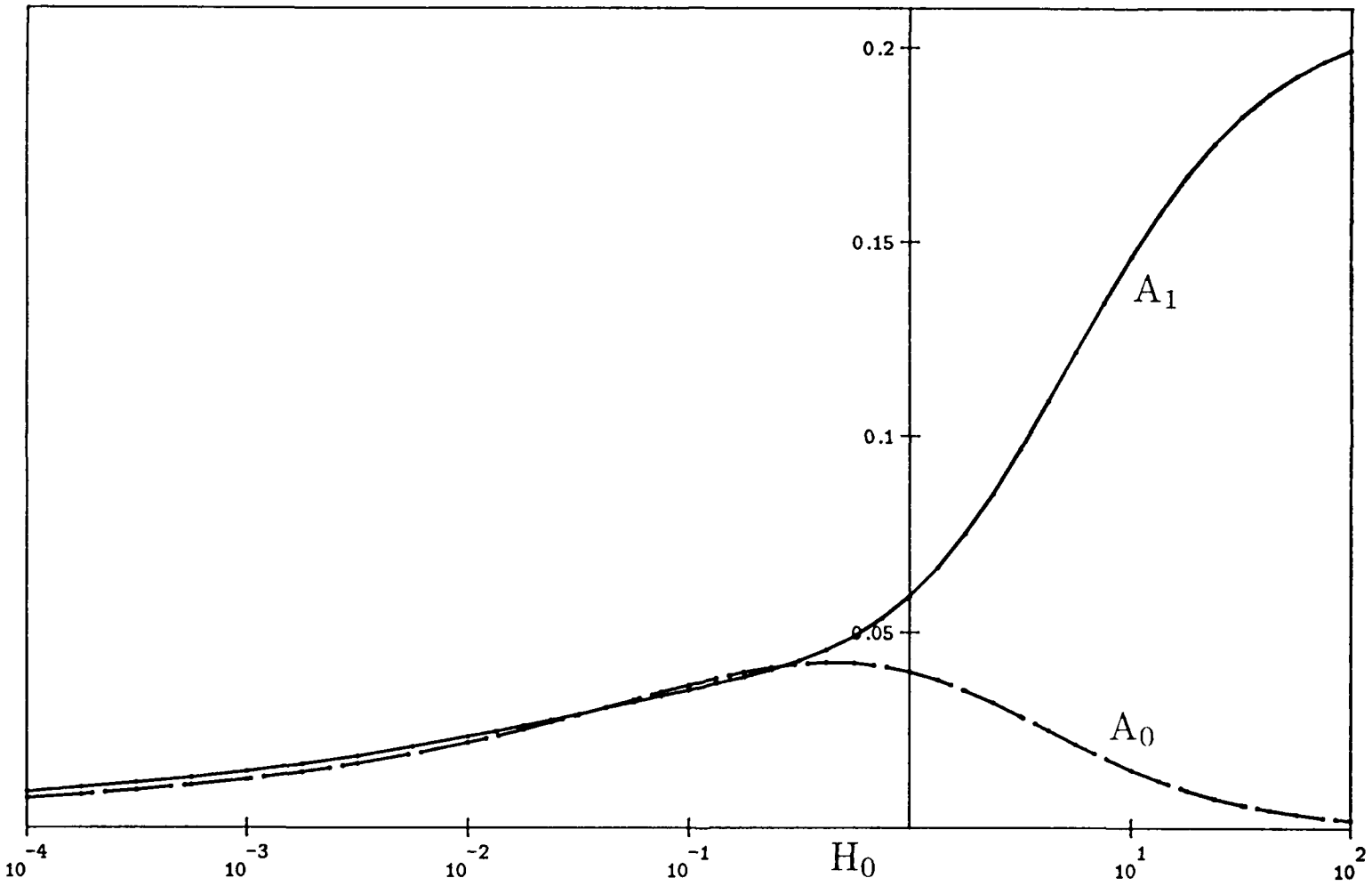

Figure 6

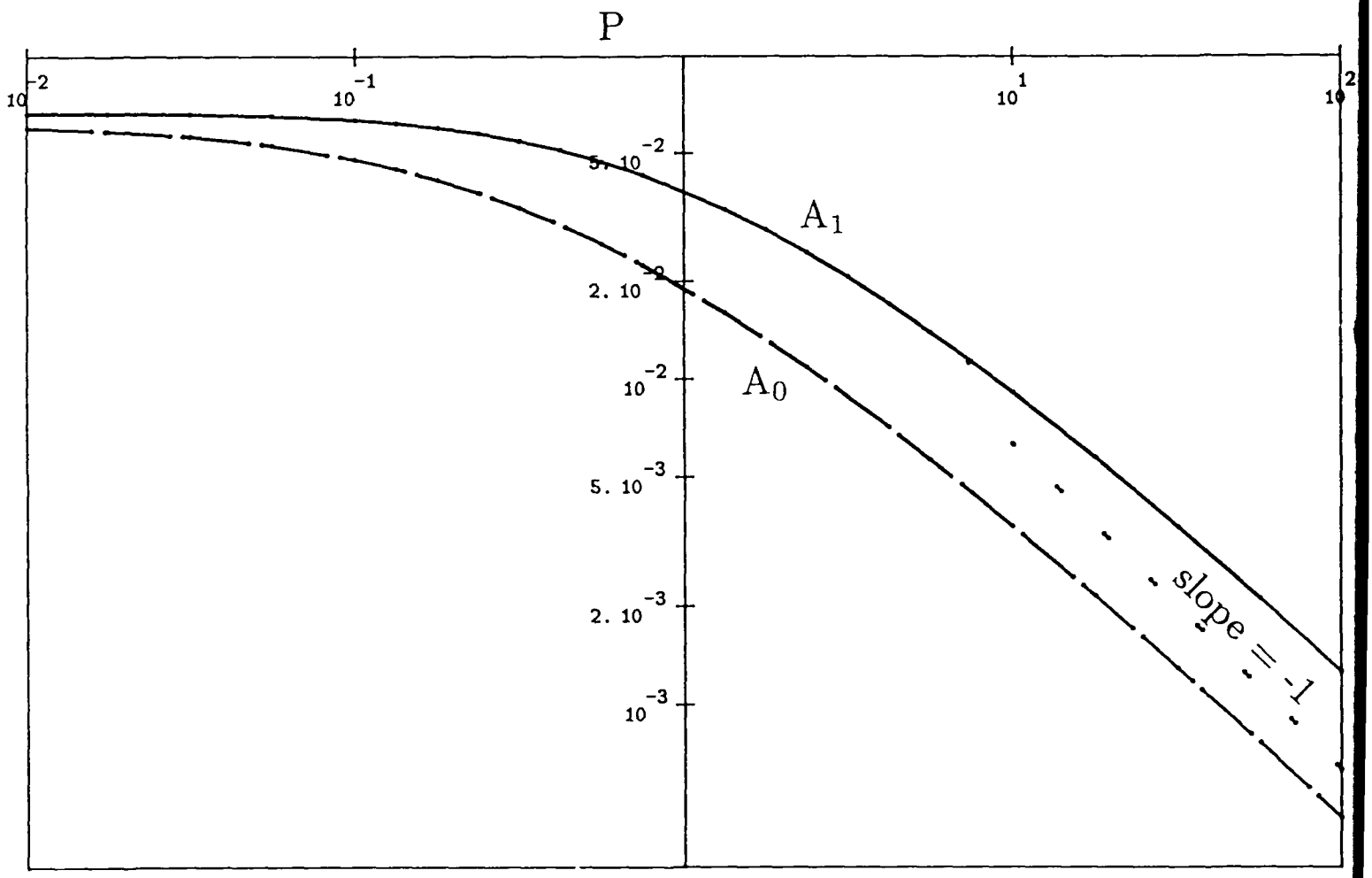

Figure 7a

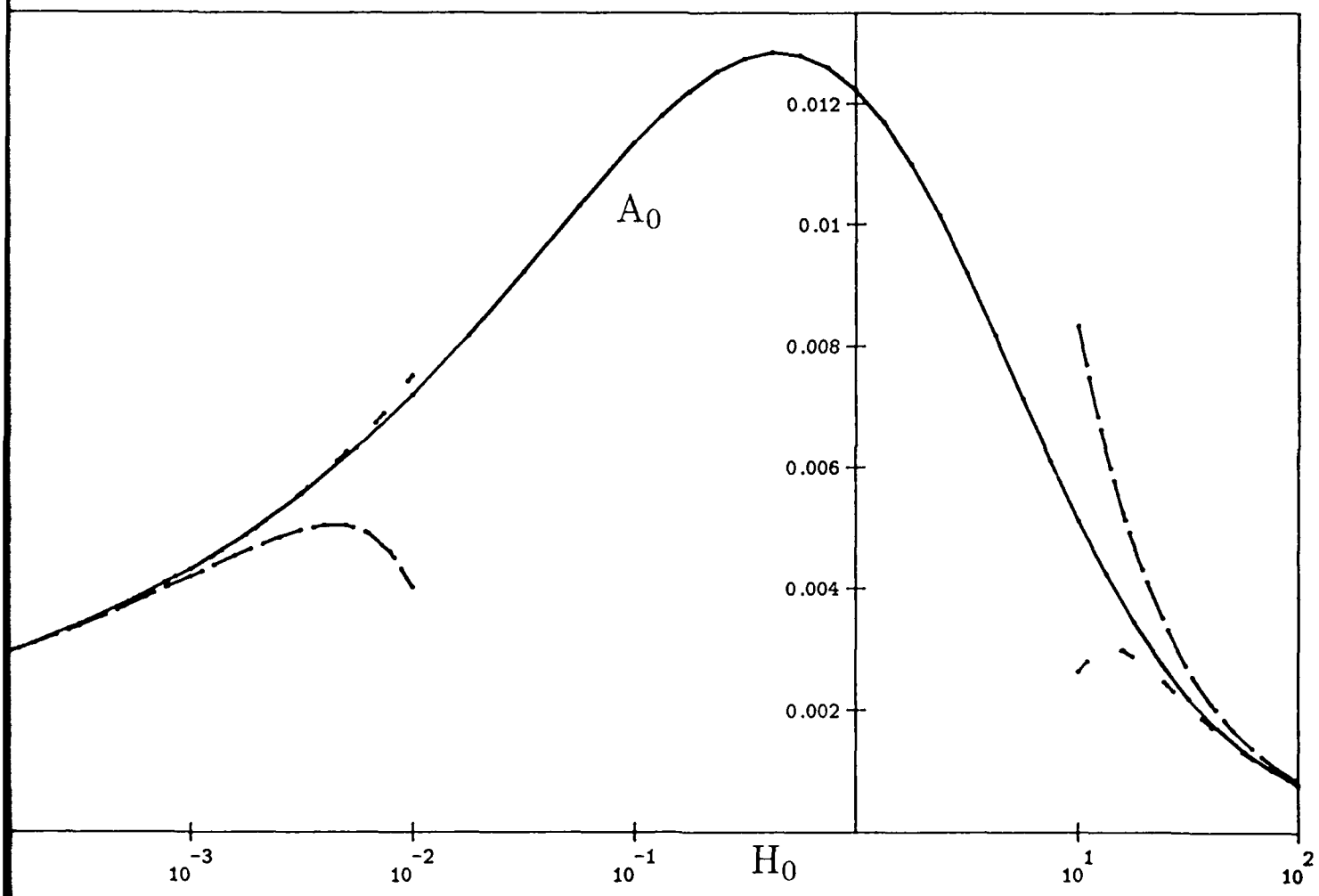

Figure 7b

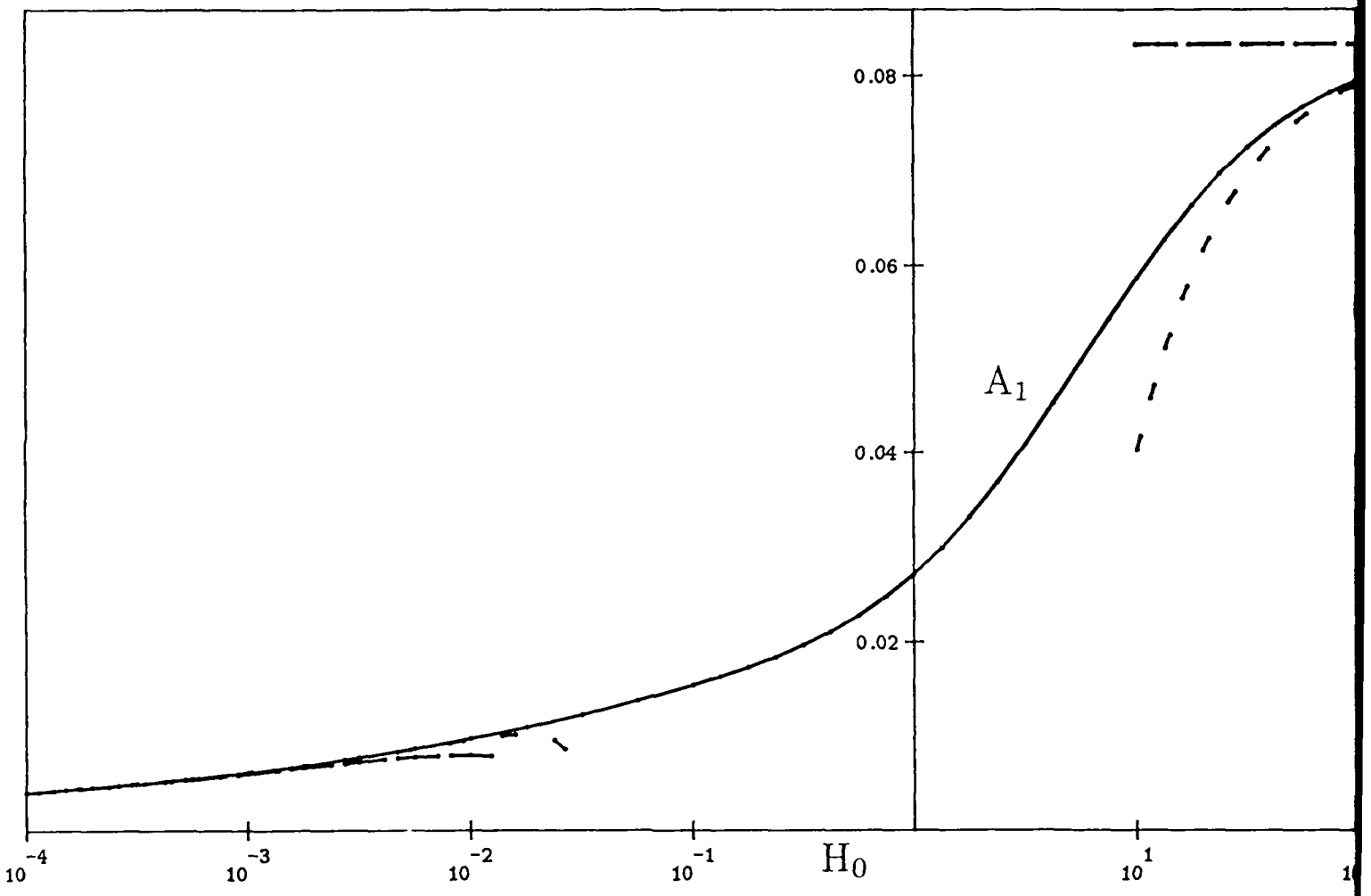

Figure 8

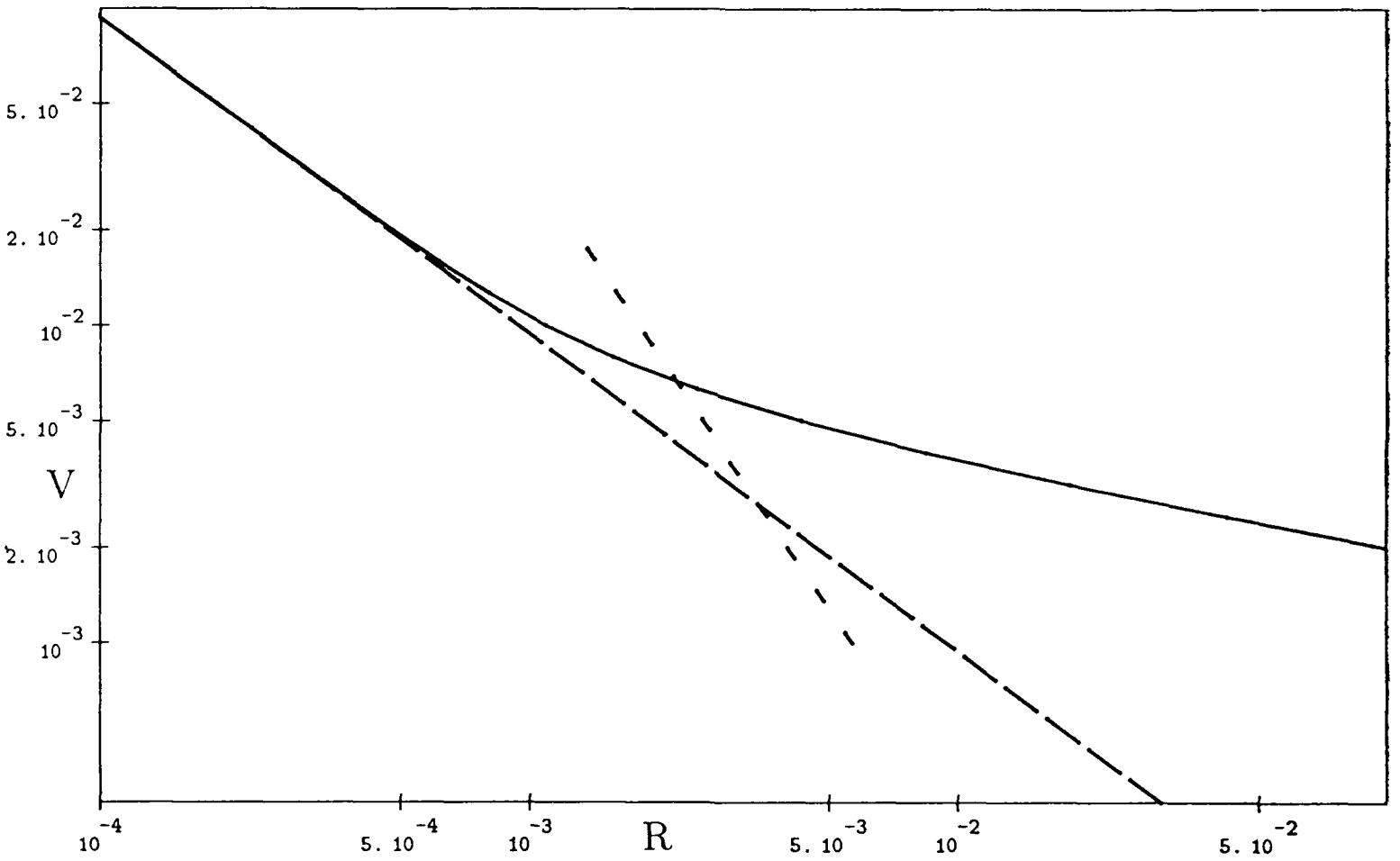

Figure 9a

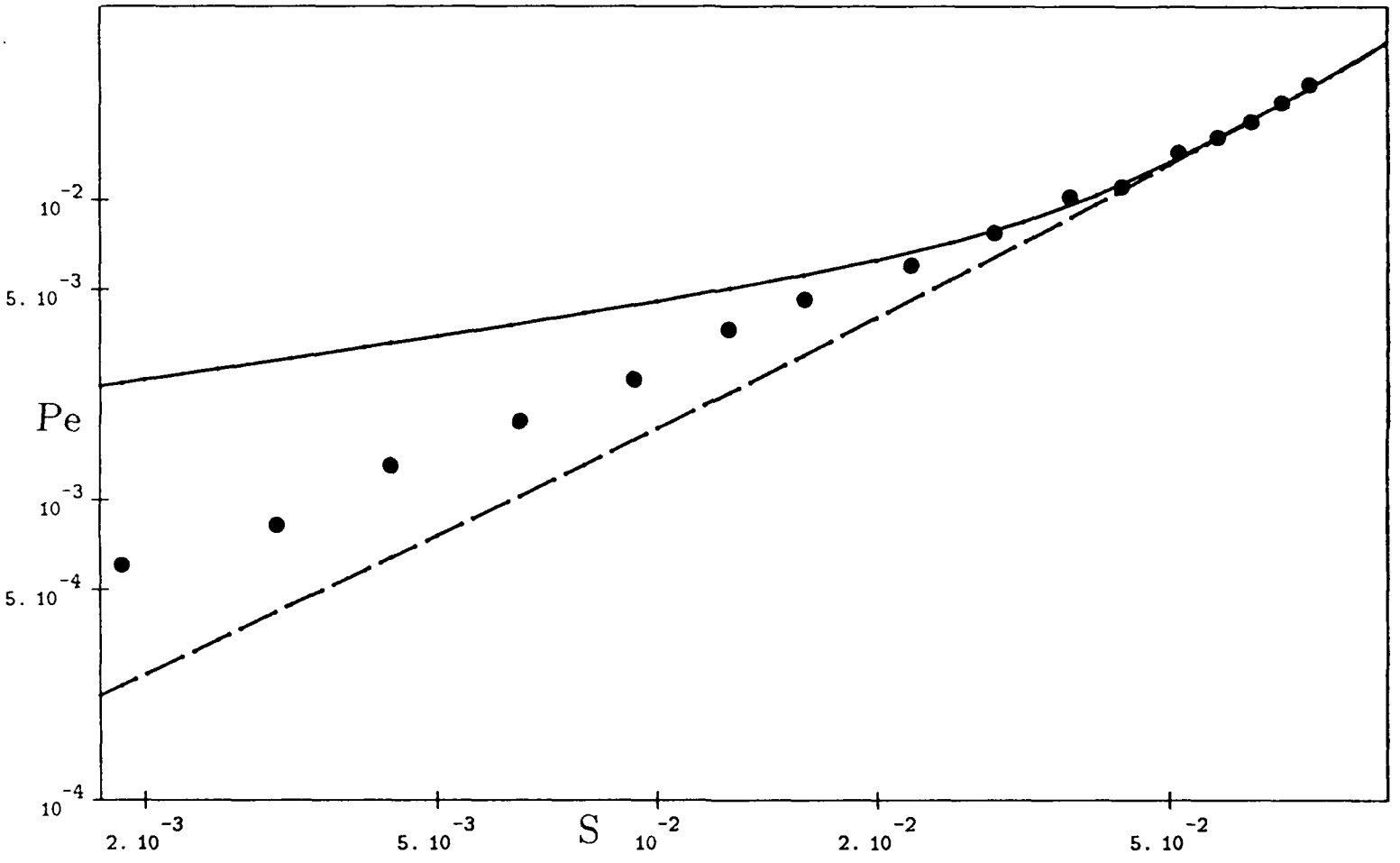

Figure 9b

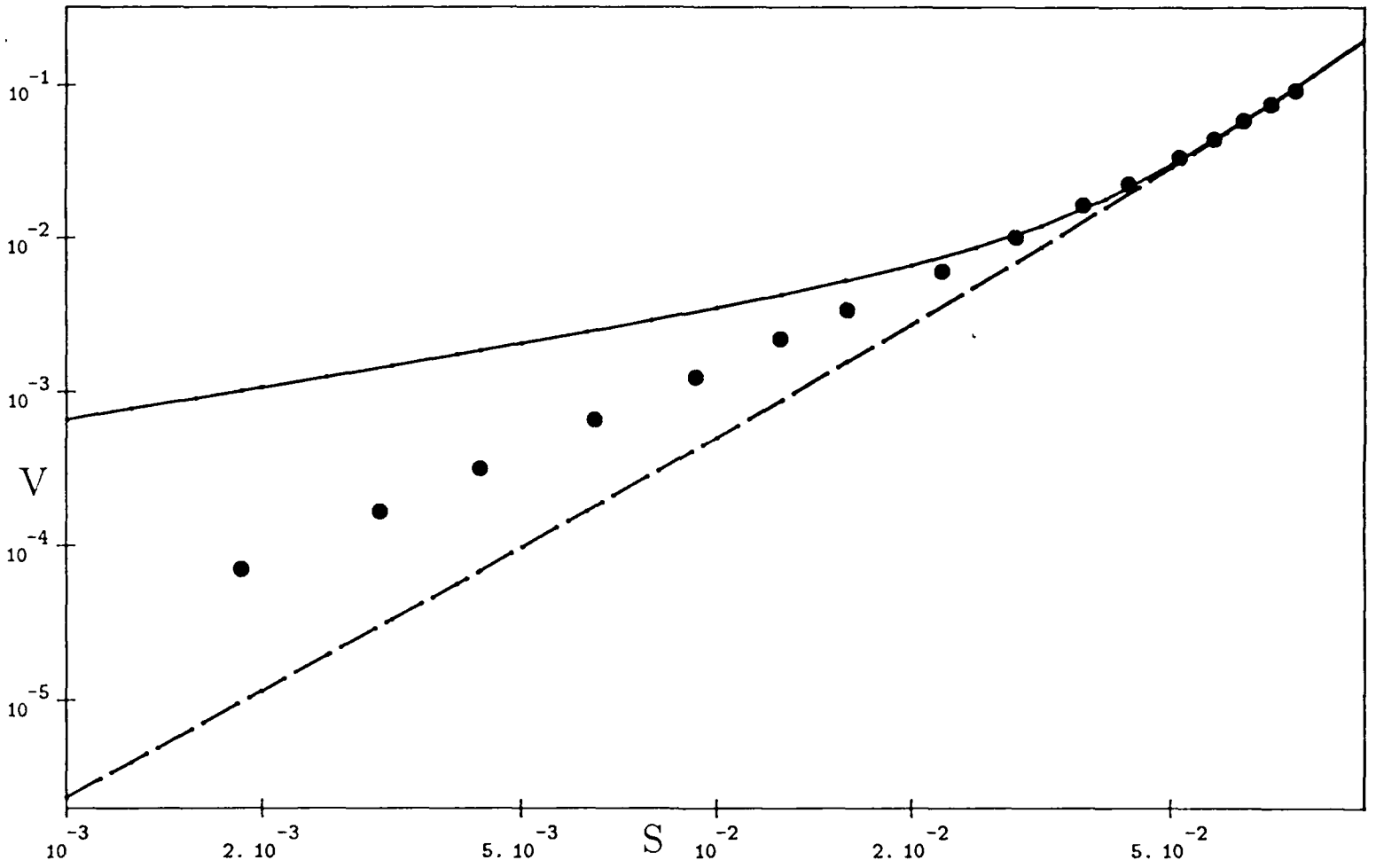

Figure 9c

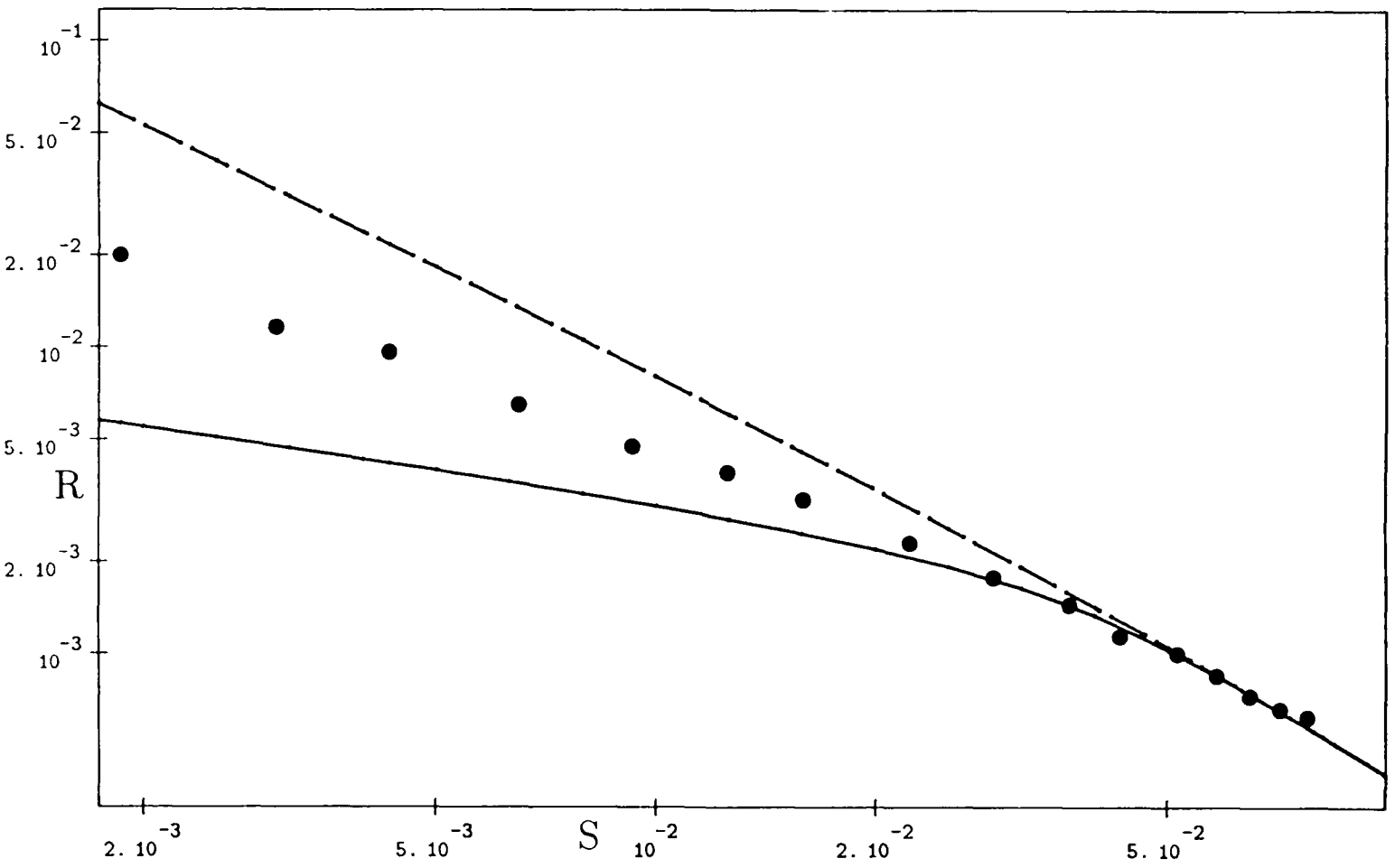

Figure 9d

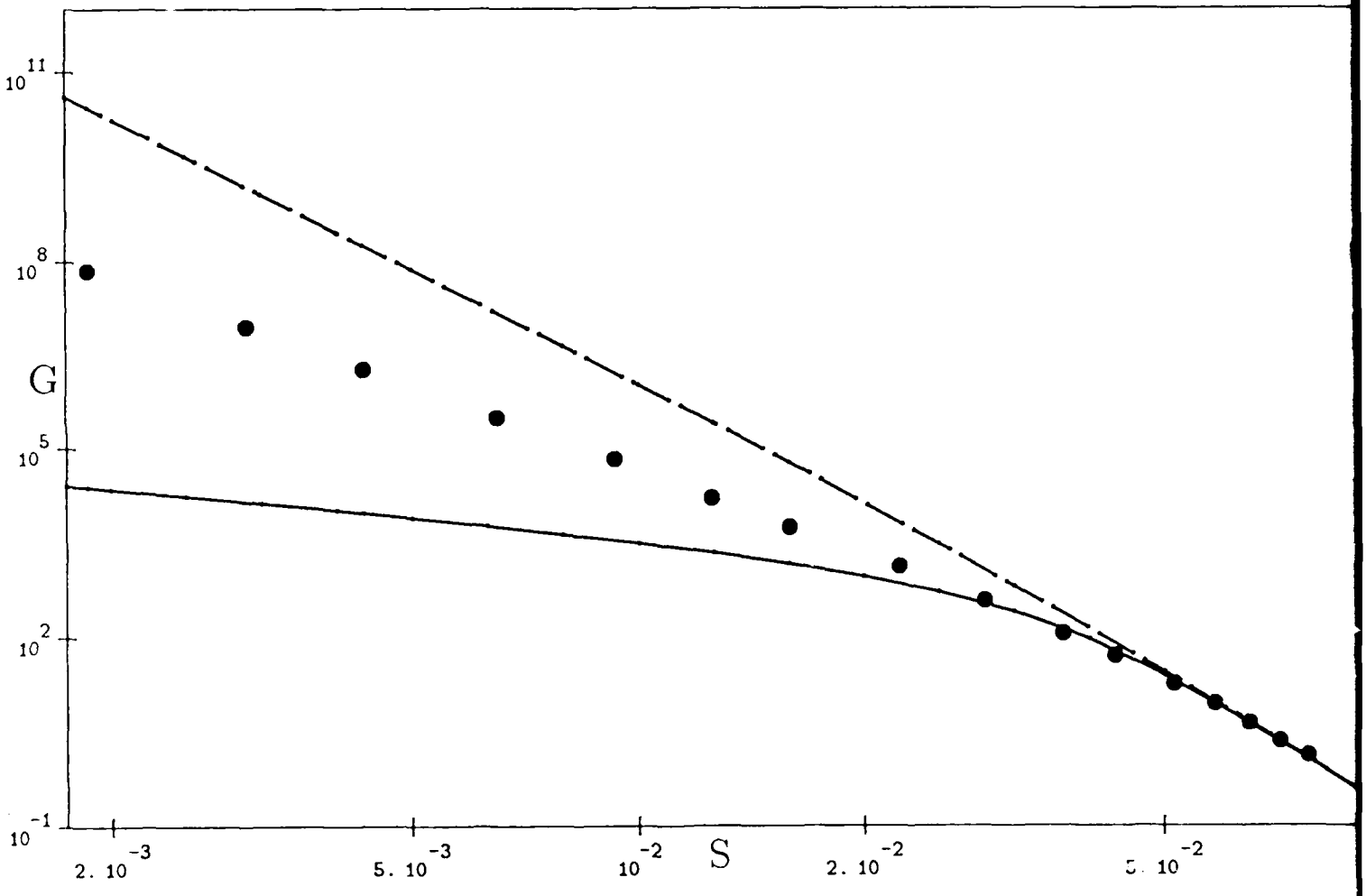

INITIAL DISTRIBUTION LIST

Defense Technical Inf. (2)
Center
Cameron Station
Alexandria, VA 22214

Library, Code 0142 (2)
Naval Postgraduate School
Monterey, CA 93943

Research Admin., Code 012
Naval Postgraduate School
Monterey, CA 93943

Department of Mathematics
Code 53/MA
Naval Postgraduate School
Monterey, CA 93943

Professor David Canright (12)
Department of Mathematics
Code 53/MA
Naval Postgraduate School
Monterey, CA 93943

Professor Y. Joshi
Mechanical Engineering Dept.
Code 69Ji
Naval Postgraduate School
Monterey, CA 93943

Professor T. McNelley
Mechanical Engineering Dept.
Code 69Mc
Naval Postgraduate School
Monterey, CA 93943

Professor Ramagopal Ananth
Chemical Engineering
Rensselaer Polytechnical Inst.
Troy, NY 12180-3590

Professor William Gill
Chemical Engineering
Rensselaer Polytechnical Inst.
Troy, NY 12180-3590

Professor Martin Glicksman
Materials Engineering
Rensselaer Polytechnic
Institute
Troy, NY 12180-3590

Professor S. C. Huang
General Electric Co.
Corporate Research &
Development Center
Bldg. 81, Room E102
Schenectady, NY 12345